MODULATION OF ANTIGEN RECEPTOR AND ONCOGENIC SIGNALING TO NF-κB BY C9ORF9

by
deMauri S. Mackie

A dissertation submitted to Johns Hopkins University in conformity with the requirements for the degree of Doctor of Philosophy

Baltimore, Maryland

February, 2016

Abstract

The adaptive immune system utilizes tightly regulated signaling networks to fight off pathogens while remaining controlled enough to avoid harmful conditions like autoimmunity and cancer. While many of the steps in antigen receptor signaling are well characterized, some of the mechanisms and proteins that are active in these pathways remain unknown. This thesis identifies a potential modulator of NF-κB signaling in the antigen receptor pathways. A protein-protein interaction screen was conducted to identify proteins which interact with the scaffolding molecule CARD11. Secondary screening of the initial hits identified C9orf9 as a potential modulator of signaling in the pathways of interest. Knockdown studies identified a specific role for C9orf9 in antigen receptor-to-NF-κB signaling, but not in antigen receptor-to-NFAT signaling or TNF-to-NF-κB signaling. Significantly, these knockdown studies also confirmed the presence of two isoforms of C9orf9 in Jurkat T cells. While it was not possible to separate the functions of the two isoforms in Jurkat T cells, knockdown of both isoforms led to changes in phosphorylation and activation of pathway proteins, which could explain the role of C9orf9 in modulating NF-κB activity. Studies in 293T cells showed that C9orf9 interacts with several members of the CARD11 signaling complex, including Bcl10. Interestingly, C9orf9 has the ability to enhance the signaling capabilities of hyperactive CARD11 variants as well as Bcl10. This was true regardless of the mechanism of action of the hyperactive CARD11 variants. A knockout mouse was generated using CRISPR/Cas9 technology in the hope that the removal of C9orf9 would lead to a defect in B and/or T cell development or activation. While this was not observed, C9orf9

knockout mice were born slightly out of Mendelian ratios in a pattern that mimics the one seen in Bcl10 knockout mice. This observation, as well as the ability of C9orf9 to associate with Bcl10, suggests that the ability of C9orf9 to modulate NF-κB signaling may hinge on the interplay between the two isoforms of C9orf9 and Bcl10. This work introduces C9orf9 into the pantheon of antigen receptor signaling proteins and suggests further questions to understand how antigen receptor signaling is regulated.

Ph.D. DISSERTATION REFEREES

Joel L. Pomerantz, Ph.D., Assistant Professor Biological Chemistry (Faculty sponsor)

William Matsui, M.D., Professor Oncology (Reader)

Table of Contents

List of Figures

Chapter 1: Introduction

Antigen receptor signaling

The adaptive immune system is a highly regulated network of cells that respond to external stimuli to produce a specific, targeted immune reaction. It defends against a wide variety of pathogens to prevent host illness. Antigen presenting cells (APCs) such as dendritic cells (DCs) process antigen from the host environment and display fragments of antigen on their surface via their major histocompatibility complex (MHC) molecules. T cells and B cells receive this information via their antigen receptors, known as B cell receptors (BCRs) and T cell receptors (TCRs). This antigen receptor signaling gets transduced through a complex system of pathways and leads to various growth and development signals. When these pathways malfunction, the immune system can react in a number of harmful ways. Innocuous antigens may be attacked, leading to allergy and autoimmunity. A harmful antigen may be ignored, which allows cancer cells to slip through the immune screening mechanisms. Or, immune cells may fail to regulate their own growth, leading to leukemias and lymphomas.

Antigen receptor activation induces the activation of many genes required for the adaptive immune response. These genes can include pro-inflammatory cytokines such as IL-2, IL-6, TNFα, and IFNγ and their respective receptors [1]. Target genes of antigen receptor signaling may also include pro-survival genes such as Bcl2 and Bim, various cell adhesion molecules, and molecules involved in antigen presentation [1]. There are several key transcription factors activated during antigen receptor signaling, including NF-κB (Nuclear Factor κB), NFAT (Nuclear Factor of Activated T cells), and AP-1 (Activator Protein 1). NF-κB is a family of critical transcription factors for the adaptive

immune response. Its targets are responsible for many of the processes just described, including cell survival and proliferation as well as effector functions like cell-specific killing. There are 5 members of the NF-κB family, including p50 (NF-κB1), p52 (NF-κB2), p65 (RelA), RelB, and c-Rel [2].

In the absence of signaling, the NF-κB dimers are bound to the protein IκBα (Inhibitor of κB alpha) and are sequestered in the cell cytoplasm [2]. Under optimal conditions, NF-κB is only released to the nucleus when IκBα is phosphorylated, ubiquitinated, and degraded as a result of antigen receptor signaling. However, because of the complex nature of the antigen receptor signaling network, there are many opportunities for proteins to malfunction and cause constitutive activation of the pathway. This removes the requirement for specific, controlled antigen receptor signals to be transduced through the pathway and allows for continuous engagement of growth and activation pathways as a result of unrestricted NF-κB activity.

CARD11 is a multidomain scaffolding protein found downstream of the antigen receptors in both B and T cells and upstream of NF-κB [3-5]. In the absence of signaling, CARD11 resides in a closed, inactive conformation. Upon antigen receptor engagement, signals are transduced through a network of proteins that lead to the phosphorylation of CARD11 by PKCθ in T cells and PKCβ in B cells [6,7]. After phosphorylation, CARD11 transitions from its closed, inactive conformation to an open, active conformation [8]. This transition is controlled by an Inhibitory Domain (ID), which interacts with the CARD (Caspase Activation Recruitment Domain), LATCH, and Coiled Coil domains and blocks recruitment of signaling cofactors to CARD11 [9,10]. In its

open state, CARD11 recruits a complex of signaling molecules to its N-terminal domains (Figure 1). These molecules include Bcl10, whose ubiquitination is required for functional signaling [11]. Other molecules recruited to the complex include the paracaspase MALT1 (Mucosal Associated Lymphoid Tissue 1), the E3 ubiquitin ligase TRAF6, the TNF-responsive signaling protein TAK1, Caspase8, and the regulatory subunit of the IKK complex IKKγ (also called NEMO) [9]. Several residues of CARD11 including S564, S567, S577, S649, and S657 can be phosphorylated by PKC, IKKβ, and at least one other kinase [6, 7, 12-14]. Phosphorylation of these residues is thought to disrupt the intramolecular binding of the ID with the CARD and coiled-coil domains, and thereby allows the protein to transition from its closed to open state.

While many of the components of the Antigen Receptor-to-NFκB pathway are known, the exact mechanism by which CARD11 signals to the IKK complex is unclear. In both T cells and B cells, the steps upstream of CARD11 are well established. In T cells, signals are received via the TCR and CD3 complex. The CD3 accessory chains are transmembrane proteins that contain cytoplasmic ITAMs (immunoreceptor tryrosine-based activation motifs) [15, 16]. After Antigen presenting cells (APCs) present antigen to the TCR, the CD3 ITAMs are phosphorylated by the kinase Lck [16, 17]. This phosphorylation allows for the recruitment of ZAP-70 (ζ-associated protein of 70-kDa), a Syk family kinase which phosphorylates LAT (Linker of Activated T cells), and SLP-76 (SH2-domain-containing leukocyte protein of 76-kDa) among other targets. LAT and SLP-76 recruit and activate many other signaling proteins that lead to activation of transcription factors and pro-survival programs [15]. PLCγ (Phosholipase C γ) is among

the proteins recruited by LAT and SLP-76. PLCγ catalyzes the separation of PIP_2 into IP_3 and DAG (diacylglycerol) [15]. While IP_3 activates calcium-based signaling pathways that activate the transcription factor NFAT, DAG phosphorylates PKC and leads to the activation of CARD11 signaling to NF-κB [18]. BCR signaling is very similar to TCR signaling.

The BCR is a membrane-bound antibody whose parent DNA has undergone V(D)J recombination to become antigen specific. At the cell surface the BCR is associated with CD79 molecules that serve a similar function to CD3 in T cells. After the BCR is activated by antigen crosslinking, the cytoplasmic ITAMs of CD79 are phosphorylated [19]. The activated ITAMs recruit the kinase Syk, the B cell correlate to ZAP-70 [20], which leads to the recruitment of PLCγ. As in T cells, PLCγ catalyzes the separation of PIP_2 into IP_3 and DAG which then go on to activate their respective signaling pathways [21].

While the steps between engagement of the antigen receptor and the phosphorylation of CARD11 by PKC are well characterized in both B and T cells, the steps downstream of CARD11 activation are somewhat less well known. Although six signaling cofactors of CARD11 have been identified, the exact mechanism by which this signaling complex activates the IKK complex is as yet unknown. I therefore hypothesize the existence of one or more previously unknown components of this pathway that may regulate CARD11 function or assist in the transduction of signals from the CARD11 complex to the IKK complex. Some of these unknown signaling cofactors may also be

relevant in DLBCL and BENTA disease and have the potential to serve as therapeutic targets in these patients.

Diffuse Large B cell Lymphoma (DLBCL) is the most common type of Non-Hodgkin's Lymphoma, comprising 30-40% of cases [22]. The three subtypes of DLBCL are the Activated B Cell –Like (ABC), Germinal Center B (GCB), and primary mediastinal B cell lymphoma. While about 50% of DLBCL cases are curable, the ABC subtype is the least responsive to treatment [23]. The ABC subtype is known for its reliance on constitutive, canonical NF-κB signaling [24]. This constitutive signaling can be caused by mutations in a number of proteins in the NF-κB pathways, including CARD11. In fact, one group found CARD11 coiled coil domain mutations in about 10% of their patient samples [25]. An immortalized cell line made from one DLBCL patient and carrying a hyperactive CARD11 mutant fails to survive in the absence of CARD11 and dies rapidly after CARD11 loss [25]. Transfection with a number of different CARD11 gain of function mutants, including its original endogenous mutant, rescues this survival phenotype and indicates that CARD11 mutants are drivers of oncogenesis in these cancers [25].

BENTA (B Cell Expansion with NF-κB and T cell Anergy) disease is a recently described condition characterized by B cell lymphocytosis and T cell anergy [26-28]. These patients have elevated numbers of mature naïve B cells but decreased memory B cells. Their CD3+ T cell numbers are lower than expected, and fail to proliferate under stimulation and have lower IL-2 secretion than healthy controls. The patients described in these papers have heterozygous germline gain of function mutations of CARD11

including C49Y, G123D, and G116S. Interestingly, the G123D mutation has also been found in DLBCL patients [29], suggesting that these mutations alone are a “first hit” and are not enough to cause lymphomagenesis without another mutagenic hit to genes in the pathway. Understanding the role of CARD11 modulators could help identify potential drug targets for DLBCL and BENTA disease.

Chapter 2: C9orf9 influences CARD11-mediated NF-κB Signaling

Protein-Protein Interaction Screen

In order to identify potential CARD11 interactors, I performed a protein-protein interaction screen using a recombinant form of CARD11. I created two different versions of CARD11, both with N-terminal V5 and myc tags and C-terminal 6xHis tags. The first version, called ΔID, contains wild type versions of the N-terminal CARD, LATCH, and Coiled Coil domains of CARD11. It serves as a truncated version of the hyperactive ΔID version of CARD11 which lacks the autoinhibitory domain and is known to have higher binding affinity for CARD11 cofactors such as Bcl10. The second recombinant version of CARD11 includes both the ID and the hyperactive L251P mutation. Although this construct contains the autoinhibitory domain, the L251P mutation is hyperactive and the construct also has higher affinity for Bcl10 than wild type CARD11 does. I hypothesized that these two constructs would specifically bind to proteins that are recruited to the CARD11 complex under hyperactive, constitutive signaling conditions and help understand the signaling pathway in oncogenic contexts. I excluded the CARD11 C-terminal PDZ-SH3-GUK domains because very little is known about the role of these domains in CARD11 signaling. I wanted to specifically identify proteins that interact with the domains of CARD11 which are known to play a role in signaling and which are known to have oncogenic mutations.

I expressed these two constructs in bacteria and used the 6X His tag to purify the protein from the lysate using nickel beads. Because CARD11 tends to precipitate out of solution, I expressed the protein in very large quantities in order to isolate enough protein for our interaction studies. I then partnered with the Johns Hopkins High-Throughput

(HiT) Center to perform a chip-based protein-protein interaction study. This technique resembles a Far Western, but is performed on a glass slide rather than on a membrane. Coated glass slides were printed with 17,000 GST-tagged proteins in duplicate, incubated with isolated rCARD11 protein, and detected with an anti—V5 antibody. A CY5-conjugated secondary antibody was used to amplify the V5-specific signal, and the chip was read on an Axon GenePix Scanner. A third chip was also incubated with the V5 and secondary antibodies to rule out any non-specific detection. GenePix Pro 6.0 software was used to analyze the fluorescent intensity of each signal and match it with the layout of the proteins printed on the chip. A protein had to have both of its printed samples fluoresce to be considered a positive hit.

The top 0.5% of fluorescent intensities for each chip were calculated and identified. Proteins with known functions unrelated to antigen receptor signaling such as tRNA synthetases were discarded from the analysis. Also eliminated were proteins which are not known to express in the immune system, but proteins which express at globally low levels throughout the body were retained. This *in silico* analysis left 63 proteins which were subjected to secondary screening. Secondary screening involved examining two different indicators of a protein's relevance to antigen receptor and CARD11 signaling. The first requirement was that it interact with CARD11, so co-immunoprecipitations were performed in HEK293T cells using cDNAs obtained from the HiT Center and our standard murine CARD11 constructs. cDNAs were obtained from our HiT Center in Entry Vectors, and Gateway cloning was used to clone each cDNA into a destination vector containing an N-terminal V5-tag. For immunoprecipitation

assays, the V5-tagged test clone was co-transfected into 293s with myc-tagged wild type, ΔID, or L251P CARD11 using the calcium phosphate method. Cells were harvested and lysed in IP lysis buffer (50mM HEPES pH7.9, 150mM NaCl, 1mM EDTA, 10% glycerol, 1% IGEPAL). The V5 tagged proteins were pulled down with anti-V5 antibodies and Protein G Sepharose beads. Lysates were run on SDS-PAGE and transferred to PVDF. Membranes were blotted with anti-V5 antibodies to detect the test proteins and anti-myc antibodies to determine the interaction with the CARD11 constructs. Test proteins which specifically interacted with hyperactive ΔID and L251P CARD11 but not wild type CARD11 were considered to be relevant for understanding hyperactive CARD11 signaling.

Finally, test proteins were evaluated on their ability to affect CARD11 signaling to NF-κB via a luciferase reporter assay. The same V5-tagged proteins were transfected into HEK293T cells (293s) along with an NF-κB responsive luciferase reporter and a constitutively active β-galactosidase construct to control for transfection efficiency and sample recovery. Each V5-tagged test construct was tested with wild type CARD11, the oncogenic mutant L251P, and a hyperactive variant of CARD11 in which the autoinhibitory domain has been deleted (ΔID). Because I was interested in understanding the mechanisms of CARD11-initiated oncogenesis, I was particularly interested in test constructs which enhanced the hyperactive variants of CARD11. The most promising candidate from the luciferase reporter assays was a small, 168 amino acid construct which significantly enhanced ΔID and L251P CARD11 activity. This construct also enhances WT CARD11 activity, although to a lesser extent (Figure 2). This construct

was identified as C9orf9, an uncharacterized gene on Chromosome 9. Very little is known about C9orf9. Sequence analysis reveals no known domains, nor any homology to other proteins. Despite this lack of domain homology, C9orf9 is relatively well conserved in higher order mammals.

C9orf9 is an enhancer of CARD11 signaling

Five shRNA constructs against C9orf9 made from sequences identified by Sigma were cloned into pLKO.1 lentiviruses and were transfected into HEK392T cells with viral packaging constructs. The resultant virions were used to infect wild type Jurkat T cells. After antibiotic selection, the ability of C9orf9 knockdown (KD) Jurkats to signal to NF-κB was assessed using the same Igκ2-IFN-luc NF-κB reporter and β-galactosidase reporter that were used in the 293 activation assays. Approximately 40 hours after transfection, cells were stimulated with αCD3 and αCD28 antibodies. C9orf9 KD cells infected with shRNA #5 (sh5) activated the luciferase reporter 50% less that control cell infected with virions containing a non-target (NT) shRNA. This effect was specific to the TCR-to-NF-κB pathway. TCR-to-NFAT and TNF-to-NF-κB signaling was not effected by C9orf9 knockdown (Figure 3).

To confirm knockdown in Jurkat T cells, cell lysates were run on SDS-PAGE and transferred to PVDF membrane. Membranes were blotted with an anti-C9orf9 antibody. Surprisingly, the lanes containing C9orf9 KD lysates were missing two bands when compared to lysates from the NT control cells (Figure 4). One of these missing bands was 19kDa, the expected molecular weight of C9orf9. The second band was 25kDa and initially inexplicable. Further study suggested that the second band actually represented a

higher molecular weight splice variant of C9orf9. This second variant was unlisted in RefSeq, so the initial interpretation of the second missing band was that it was due to post-translational modification of the 19kDa species of C9orf9. However, in searching for a cDNA of C9orf9 that contained UTRs, I found a construct claiming to express a 222 amino acid version of C9orf9 (approximately 25kDa and the size of the inexplicable band). Interestingly, the reference link for this new cDNA connected to a RefSeq entry that had been replaced with the 168aa version of C9orf9. Comparison of the two constructs and an analysis of the genomic locus indicated that Jurkat T cells did express both of these variants of C9orf9. These two variants have their 165 N-terminal amino acids in common, but differ in their C-termini. Failure of the mRNA to splice its fourth exon leads to the 222aa variant. The 168aa variant is the result of mRNA splicing that removes a significant portion of the transcript and induces a frame shift. That is to say, the entire coding region of the 168aa variant is contained in the transcript of the 222aa variant (Figure 5A). The fifth exon of the 168aa variant is actually entirely present in the 3'UTR of the 222aa variant. Because shRNA targets transcripts at the mRNA level and leaves the endogenous DNA intact, it was impossible to design an shRNA hairpin that targeted only the 168aa variant of C9orf9 (Figure 5B). ShRNA that targeted only the long form of C9orf9 were not effective at limiting anti-CD3/anti-CD28-induced NF-κB signaling in Jurkats as shRNA that targeted both forms, suggesting that both forms are required for signaling (Figure 5C).

This hypothesis was confirmed when I attempted to rescue the C9orf9 sh5 knockdown cells luciferase activation phenotype using only one shRNA-resistant C9orf9

construct. Attempts to use either the 168aa variant or the 222aa variant both failed to rescue this phenotype. Many attempts to rescue the phenotype using both constructs were initially unsuccessful (Figure 6A). Changing the ratio of long:short C9orf9 had no effect on the constructs' ability to rescue the phenotype (Figure 6B). Pre-infecting Jurkat cells with virions encoding the shRNA-resistant rescue constructs before knocking down C9orf9 with shRNA containing virions was also ineffective (Figure 6C). What was ultimately successful was using a pseudo-polycistronic vector which contains viral 2A sequences and allowed us to express both C9orf9 constructs under the same, very strong promoter. The pULTRA vector contains the very strong human poly-ubiquitin promoter upstream of GFP, two viral 2A sequences, and two multi-cloning sites. Viral 2A sequences are named for their host viruses, ie P2A for Porcine teschnovirus 1 and T2A for *Thosea asigna* virus. They are short, 18-22aa sequences that utilize a sequence of conserved prolines to induce ribosomal skipping. In essence, the presence of these prolines bends the nascent amino acid chain such that the ribosome is unable to complete the amino acid peptide linkage and ultimately generates separate peptide oligomers during the same readthrough. By using both 2A sequences in the pULTRA vector, I was able to express GFP, long C9orf9, and short C9orf9 in the same plasmid and under the same promoter. Interestingly, the orientation of the two C9orf9 variants in the vector was relevant because in the N-GFP-short C9orf9 –long C9orf9-C construct, the ribosomal skipping did not always occur, leading to the presence of one combined peptide of short + long C9orf9 (Figure 7A). This construct failed to rescue the C9orf9 knockdown luciferase assays. Contrastingly, the GFP-Long C9orf9 – short C9orf9 construct

generated the expected expression of distinct GFP, long C9orf9, and short C9orf9. This construct was able to rescue the activation phenotype in C9orf9 KD Jurkats (Figure 7B).

Once it was identified that two C9orf9 constructs exist, both were tested for their ability to affect signaling in HEK293T cells. Constructs expressing either the long or short form of C9orf9 enhanced CARD11-mediated activation of Igκ$_2$-IFN-Luc, the NF-κB responsive luciferase reporter, in HEK293T cells. All forms of CARD11, both WT and hyperactive, were subject to this enhancement. The mechanism of CARD11 hyperactivity had no bearing on this enhancement and CARD11 mutants that decrease CARD11 inhibitory domain (ID) mediated auto inhibition, such as ΔID, C49Y, L251P, F123I, and L225LI, as well as CARD11 mutants that have enhanced Bcl10 recruitment, such as C49S, Y98F, and T117A [10] were affected by C9orf9 expression (Figure 8A-E).

In an attempt to determine which regions of C9orf9 affect signaling, and to understand the biological relevance of having two splice variants expressed, truncation constructs of C9orf9 were made and named for their terminating residues. The H165 construct expresses only the 165aa which are common to both the full length long and short isoforms of C9orf9. Two other constructs are truncations of the long isoform and terminate at the Q189 and K206 residues, respectively (Figure 9). When these constructs were tested in the 293 NF-κB luciferase reporter activation assay, K206 truncation enhanced wild type CARD11 signaling more than any of the other truncations, but less than full length long C9orf9. The Q189 and H165 truncations did not enhance wild type CARD11 signaling in this assay, but neither did short C9orf9, which typically enhances wild type CARD11 signaling between 1.5 and 3-fold (Figure 10A).

In the version of this assay using hyperactive L251P CARD11, similar results were seen. The K206 truncation enhanced CARD11 L251P signaling to similar levels as the full length long form of C9orf9, even at a lower protein expression level. In the same assay, the Q189 truncation enhanced L251P CARD11 signaling two fold, while the H165 truncation enhanced L251P signaling almost 3 fold, the same as full length short C9orf9 (Figure 10B).

C9orf9 interacts with CARD11 cofactors

To determine which, if any, CARD11 cofactors interact with C9orf9, I performed immunoprecipitations of these proteins in 293T cells. Cells were transfected with FLAG-tagged cofactors and untagged C9orf9. Anti-FLAG antibodies were used to pull down protein complexes onto Protein G sepharose beads, and the complexes were then eluted with FLAG peptide.

The first cofactor I examined was Bcl10, which is the most relevant to signaling as well as the most well characterized co-factor. Interestingly, the full length long and short forms of C9orf9 interacted with Bcl10, as did the K206 truncation construct and the H165 construct. The Q189 construct did not interact with Bcl10. It may be that there is an element between residues H165 and Q189 which inhibits the interaction between C9orf9 and Bcl10, but which is "buried" in the full length version of the protein (Figure 11A). I next examined C9orf9 interaction with NEMO (IKKγ) and found the same results. Only the version of C9orf9 which terminates at reside Q189 failed to demonstrate and interaction with NEMO-FLAG (Figure 11B). Similar results were also obtained when I investigated C9orf9 interaction with TAK1 (Figure 11C).

C9orf9 knockdown decreases phosphorylation of pathway proteins

Many proteins in the TCR-to-NF-κB pathway are activated by phosphorylation (Figure 12) [30], and many of these phosphorylation events are detectable via Western blot by phospho-specific antibodies. If C9orf9 is influential in this pathway, I would expect that phosphorylation of pathway proteins will be decreased in C9orf9 knockdown Jurkat cells when compared to control cells. In these experiments, cells were stimulated with anti-CD3 and anti-CD28 antibodies at 37°C for the indicated lengths of time. Cells were harvested and lysed in IP lysis buffer plus protease inhibitor cocktail then run on SDS-PAGE and analyzed by Western blot (Figure 13). Analysis of PKCθ phosphorylation at residue T538 also showed decreased phosphorylation in the C9orf9 knockdown cells as compared to control cells. IκBα phosphorylation was also decreased, but to a lesser degree than PKCθ phosphorylation. In normal signaling, the phosphorylation and subsequent degradation of IκBα is what allows NF-κB to translocate to the nucleus and begin signaling. I therefore analyzed degradation of total IκBα. I did not see the clear lack of IκBα degradation we would expect with the decreased levels of NF-κB signaling we measure by luciferase assay and the clear differences in phosphorylation we observe higher in the TCR-to-NF-κB pathway.

C9orf9 knockdown does not lead to cell death in OCI-LY3 DLBCL cells

OCI-Ly3 cells are a cell line derived from Activated B Cell Diffuse Large B Cell Lymphoma (ABC DLBCL) patient samples. They contain an endogenous allele of the L251P mutation of CARD11 and require CARD11 for survival [25]. I hypothesized that because C9orf9 appears to be an enhancer of CARD11 signaling in 293T cells and Jurkat

T cells it would also play a role in CARD11-mediated survival of OCI-Ly3 DLBCL cells. Virions containing the pSRGN vector with C9orf9 shRNA and packaged with pCL-Eco were made in 293T cells and used to infect OCI-Ly3 cells expressing the ecotropic receptor mCAT1. A non-target shRNA was used as a negative control and an shRNA targeting CARD11 was used as a positive control. In this system, cells infected with the pSRGN vector will express GFP and be detectable in the FITC channel of a flow cytometer. By tracking the percent of live cells which are GFP positive, conclusions can be drawn about the effects of the shRNA expressed by the pSRGN vector on cell survival. OCI-Ly3 cells infected with a CARD11-targeting shRNA will die within 7-14 days, while 90% of cells infected with the non-target hairpin will survive. Surprisingly, I was unable to demonstrate a significant difference in cell survival between cells infected with the non-target hairpin and cells infected with the C9orf9 targeting hairpin (Figure 14). Several possibilities exist to explain this result. First, the shRNA may not successfully target C9orf9 in OCI-LY3 cells. Although Western blotting of sorted GFP positive cells could show that the C9orf9 hairpin is effective at knocking down protein in surviving cells, in the case of a partially effective hairpin, a result of C9orf9 expression in the sorted cells would not confirm the lack of a requirement of C9orf9 for cell survival, as the cells in which C9orf9 was knocked down could be dead and therefore not able to be isolated by cell sorting. Because of the potentially inconclusive nature of the assay, cell sorting and subsequent Western blotting for C9orf9 in C9orf9 KD OCI-Ly3 cells was not performed. Secondly, the role of C9orf9 on OCI-Ly3 cell survival may be more of a modulating role than a requirement for survival; in this case, the effect of C9orf9

knockdown on survival might be subtle enough as to not appear significant in this assay. Third, C9orf9 may play no role in CARD11-mediated cell survival of OCI-LY3 cells. Given the current data, it is impossible to distinguish which of these possibilities is true in the described assay.

C9orf9 knockout mouse CRISPR design and characterization

The CRISPR/Cas9 system has drastically shortened the length of time required to make knockin and knockout mice. In connection with the JHMI Transgenic Mouse Core, I made use of this new technology to design and create a C9orf9 global deletion mouse. I targeted the second exon of mouse C9orf9, on Chromosome 2, which contains the start methionine and initial coding region of C9orf9 (Figure 15). It is important to target an upstream region of a gene when using CRISPR because if a more downstream region is left intact, the resultant message may be too long to be degraded by nonsense-mediated decay. Using the Zhang lab's website (crispr.mit.edu), I identified several potential PAMs (protospacer adjacent motifs) with low probabilities of off-target effects. I chose one that would target a region approximately 10 amino acids downstream of the start codon, which I hoped would maximize the probability of nonsense mediated decay of any resultant transcript. Instead of relying solely on non-homologous end joining (NHEJ) to repair the double stranded break induced by Cas9 and introduce helpfully disrupting mutations, I opted to use a long oligo to achieve homologous recombination. Using this oligo, I inserted an AvrII site (CCTAGG) into the protospacer of the repaired DNA. This achieved several goals: First, I inserted an inframe stop codon ten amino acids downstream of the start codon. Second, by adding a restriction site, I was easily able to

confirm the presence of the stop codon during genotyping. Finally, by inserting the restriction site in the middle of the protospacer, I ensured that any residual Cas9 protein in the embryonic cells can't target the repaired DNA.

To create the necessary constructs for embryonic injection, I followed the Jaenisch group methodology [31]. Using their PX330 construct which contains the sequences for both Cas9 and the sgRNA/tracr chimera, I inserted my specific protospacer and generated RNA for both constructs. I used a 126bp DNA oligo to induce homology-directed repair (HDR). The injection mixture contained 25ng/µL (2µg total) Cas9 mRNA, 1µg sgRNA, and 2µg DNA oligo in 80ul H_2O and was injected into single cell C57/Black 6 embryos by the JHMI Transgenic Mouse Core.

To genotype the resultant embryos, I isolated DNA from ear punches using ethanol precipitation and amplified a 640bp region of chromosome 2. Overnight digestion of the entire PCR product with AvrII generated a 414 bp fragement and a 228 bp fragment in alleles with the AvrII site from HDR. I was easily able to distinguish homozygous knockout mice by their lack of the initial 640bp amplified product as both copies were digested. Heterozygous individuals displayed all three potential DNA fragments, and DNA from homozygous wild type individuals remained uncut with only the resultant 640bp fragment (Figure 16).

Although several of the initial pups had the desired recombination as indicated by the presence of the AvrII site, only one of these individuals achieved germline transmission and passed the disrupted C9orf9 allele to its offspring. The existence of mice which displayed evidence of recombination in DNA taken from ear punches, but

which failed to achieve germline transmission of the mutation, can be attributed to mosaicism caused by delayed or incomplete action of the Cas9 during early embryonic development. It is impossible to predict whether Cas9 will be effective in the single cell embryo or in one or more of the daughter cells at the next stages of embryonic development, so it is important to always consider the possibility of mosaicism in the initial mouse pups. Having more pups born will increase the odds of getting germline transmission of your targeted gene. It is also important to test for expression of your targeted protein in multiple tissues if possible (in the case of a global deletion such as this). This will confirm that the target mutations are present in the DNA in multiple cell types and that the resultant mRNA transcript is being degraded consistently across cell types. In this case, Western blotting of mouse testes, where C9orf9 is most highly expressed, demonstrated a clear lack of protein expression of the short isoform of C9orf9 in the C9orf9 KO mice (Figure 17).

To assess the role of C9orf9 knockdown in the murine immune system, immune system development and B and T cell activation were analyzed via flow cytometry. All experiments were performed in 7-12 week old mice. When compared to wild type mice, splenic T cell numbers in C9orf9 KO mice were grossly normal. There were no significant differences in total CD3 positive cells, CD4 single positive cells, or CD8 CD positive cells. Numbers of CD4+CD25 double positive Treg cells were also normal (data not shown). CD4+CD25- cells were stratified on CD44 and CD62L to identify naïve, memory, and effector subsets as described [32]. There were no significant differences among these subsets, indicating that splenic T cell development in C9orf9 KO mice is

grossly normal (Figure 18B). Thymic T cell development in C9orf9 KO mice was also determined to be normal. Cells isolated from the thymus of 8-10 week old mice were stained for CD3, CD4, and CD8. Because T cells undergo development and differentiation from CD4-CD8- through CD4+CD8+ to CD4 and CD8 single positive stages in the thymus, I looked at the relative numbers of each of these subsets and found them to be normal. CD4-CD8- cells go through four developmental stages, termed DN1-4, in the thymus. These stages can be identified by the surface expression of CD25 and CD44, starting with CD44+CD25- (DN1), moving through CD44+CD25+ (DN2), to CD44-CD25+ (DN3), and ending with CD44-CD25- (DN4). All for DN stages were normal in C9orf9 KO mice when compared to gender and age matched WT controls (Figure 18A).

Splenic and bone marrow B cell development were also assayed by flow cytometry. B cell development is divided into several stages depending on the status of V(D)J recombination of the heavy and light chains of the Ig locus. The variable region of the heavy chain locus is made up of many V, D, and J segments that can be recombined in different ways to create antibody diversity. These joins are also accompanied with nucleotide insertions to increase the level of diversity of the recombined fragments. V(D)J recombination starts at the heavy chain locus with an initial D-J join which is followed by a V-DJ join. The resultant heavy chain is transported to the cell surface to be tested for functionality alongside the surrogate light chain. Once a function heavy chain has been made, recombination of the light chain begins. These various stages of B cell development have been named and are also accompanied by up and downregulation of

additional cell surface markers. Pre-pro Bs, Pro Bs, Pre Bs, and Immature Bs, can be identified by their expression of B220, CD19, CD43 and IgM according to the following chart in Figure 19A [33].

Bone marrow tissue was isolated from C9orf9 KO and age and gender-matched WT mice Single cell suspensions were made and stained for the appropriate B cell markers. Cells were initially stratified on B220 and CD19. B220+CD19- cells were then stratified on CD43 and IgM. B220+CD19-CD43+IgM- cells were classified as pre-pro B cells. B220+CD19+ cells were also then stratified on CD43 and IgM. B220+CD19+CD43+IgM- cells were classified as proB cells. B220+CD19+CD43-IgM- cells were classified as preBs, and B220+CD19+CD43-IgM positive cells were classified as immature B cells. All of the described subsets were indistinguishable between C9orf9KO mice and WT mice, indicating no significant differences in bone marrow B cell development between genotypes (Figure 19B). Splenic B cells were also analyzed for makers of development and differentiation. In one scheme cells were stained with antibodies against CD23, CD21, and IgM. Four different developmental stages were examined based on these markers. Marginal zone B cells were defined as being CD23-CD21+IgM+. Transitional 1 cells were defined as CD23-CD21-IgM+. Transitional 2 cells were defined as CD23-CD21+IgM+. Finally, mature follicular zone B cells were defined as being CD23-CD21-IgMlow [34]. There were no differences in these stages of differentiation between C9orf9 KO mice and WT mice (Figure 20A and B).

Splenic B and T cells were also analyzed for their ability to upregulate activation markers and to proliferate in response to stimuli [35,36]. Splenic B cells were isolated

using the MACS Pan B cell Kit II (Miltenyi). Cells were stained with 2µM CFSE Invitrogen CellTrace CFSE. 10µg/mL anti IgM, or 20 µg/mL LPS were used to stimulate the B cells. Proliferation was measured by change in MFI after 72 hours incubation at 37°C in 5% CO_2 and 95% humidity. C9orf9 KO B cells proliferated similarly to WT B cells upon stimulation (Figure 21A). Activation was also measured by the upregulation of cell surface markers after 24 hours of the described stimuli. There was no difference in the upregulation of CD86, MHC Class II, or CD25 in C9orf9 KO B cells as compared to WT B cells (Figure 21B) [35, 36].

T cells were analyzed in a similar fashion to B cells to determine their responses to stimuli. CD4 and CD8 T cells were isolated using the MACS CD4 and CD8 negative selection kits (Miltenyi). Cells were stained with 1µM CFSE. Cells were stimulated using 3µg/mL plate bound anti-CD3 in the presence or absence of 2µg/mL soluble anti-CD28. Proliferation was measured by change in MFI after 72 hours incubation at 37°C in 5% COC in 5% CO_2 and 95% humidity. C9orf9 KO T cells proliferated similarly to WT T cells upon stimulation (Figure 22A). Activation was also measured by the upregulation of cell surface markers after 24 hours of the described stimuli. There was no difference in the upregulation of CD25, CD44, or CD69 in C9orf9 KO CD4T cells as compared to WT CD4T cells (Figure 22B) [37].

I also tracked gentoypes of the offspring born from het-het crosses. Of 137 pups born, 39 pups (28%) were WT, 72 (52%) were heterozygous, and 26 (19%) were C9orf9 KO. This is slightly out of the expected Mendelian ratio of 25%-50%-25%. Interestingly, this pattern mimics that seen in an early description of Bcl10 KO mice [37].

In their system, about 1/3 fewer Bcl10 KO mice were born than were expected. Day E10.5 fetal mice were extracted and were found to have significant neural tube defects which lead to embryonic lethality. It is possible, given the interaction between Bcl10 and C9orf9 *in vitro* that a defect in C9orf9 may lead to the same type of embryonic defect seen in the absence of Bcl10.

Figure 1

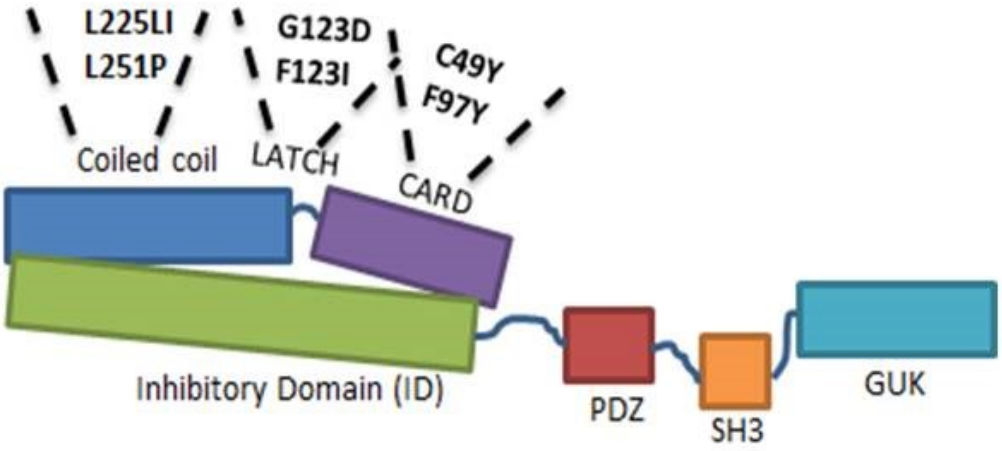
L225LI
L251P
G123D
F123I
C49Y
F97Y
Coiled coil
LATCH
CARD
Inhibitory Domain (ID)
PDZ
SH3
GUK

Figure 2

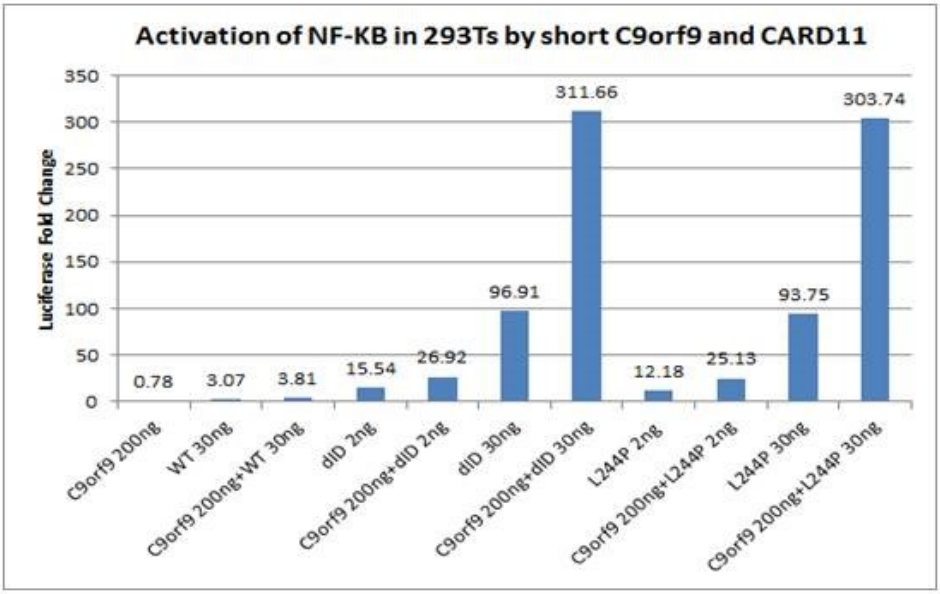
Activation of NF-KB in 293Ts by short C9orf9 and CARD11
Luciferase Fold Change
350
300
250
200
150
100
50
0
0.78
3.07
3.81
15.54
26.92
96.91
311.66
12.18
25.13
93.75
303.74
C9orf9 200ng
WT 30ng
C9orf9 200ng+WT 30ng
dID 2ng
C9orf9 200ng+dID 2ng
dID 30ng
C9orf9 200ng+dID 30ng
L244P 2ng
C9orf9 200ng+L244P 2ng
L244P 30ng
C9orf9 200ng+L244P 30ng

Figure 3

A

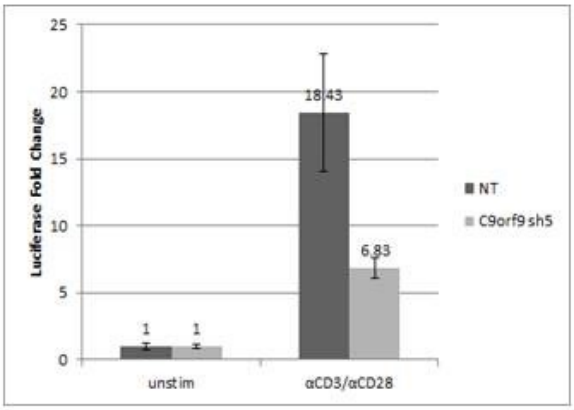
Luciferase Fold Change
25
20
15
10
5
0
18.43
6.83
1
1
unstim
αCD3/αCD28
NT
C9orf9 sh5

B

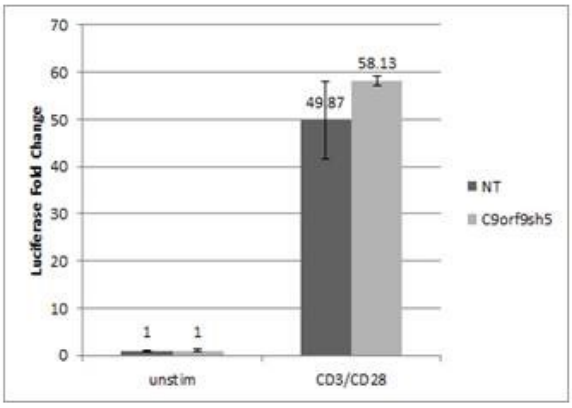
Luciferase Fold Change
70
60
50
40
30
20
10
0
58.13
49.87
1
1
unstim
CD3/CD28
NT
C9orf9sh5

C

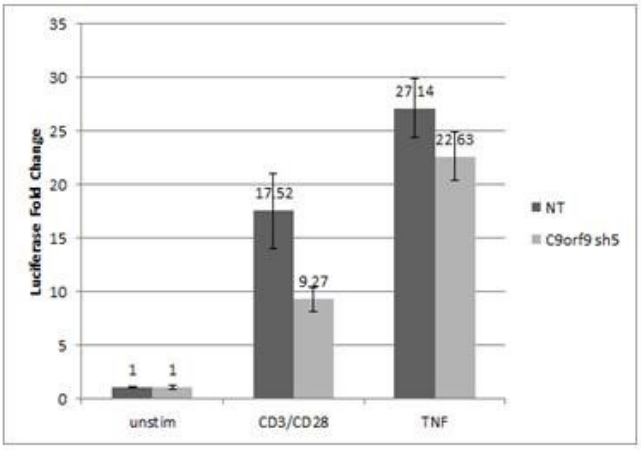
Luciferase Fold Change
35
30
25
20
15
10
5
0
27.14
22.63
17.52
9.27
1
1
unstim
CD3/CD28
TNF
NT
C9orf9 sh5

Figure 4

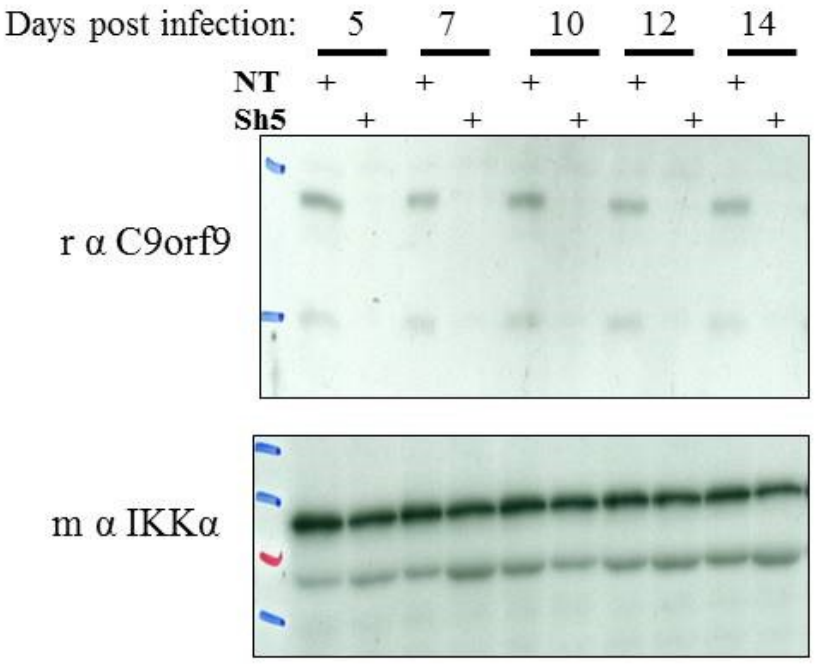

Figure 5

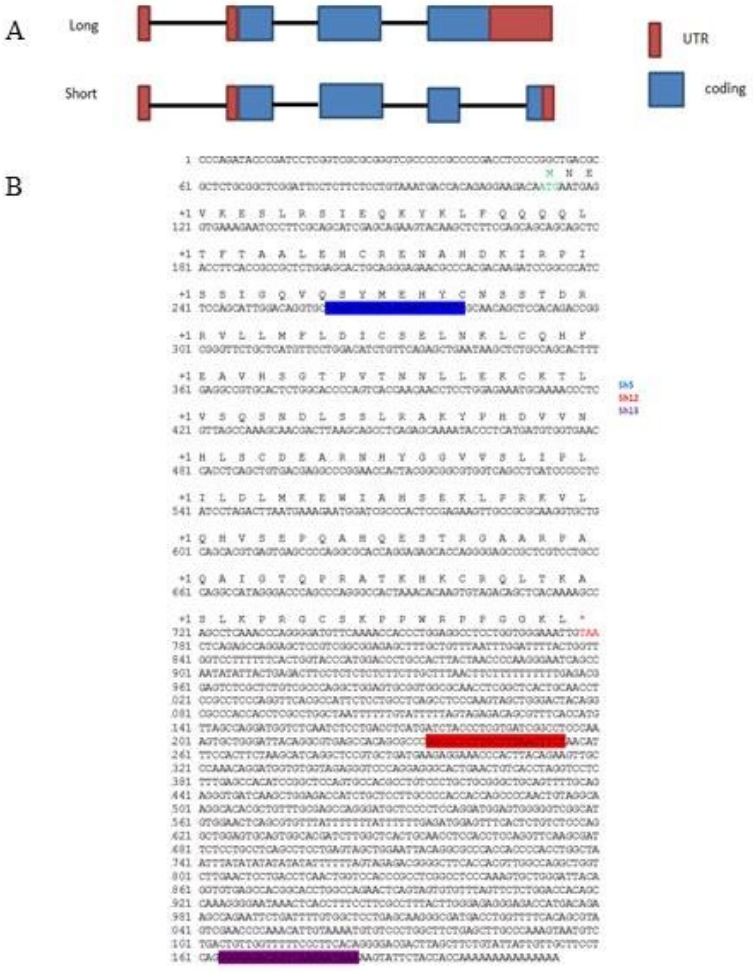
A
Long
Short
UTR
coding
B
C
Luciferase Fold Change
14
12
10
8
6
4
2
0
10.62
9.35
8.79
4.78
1
1
1
1
NT
C9orf9 sh5
C9orf9 sh12
C9orf9 sh13
unstim
αCD3/αCD28

Figure 6

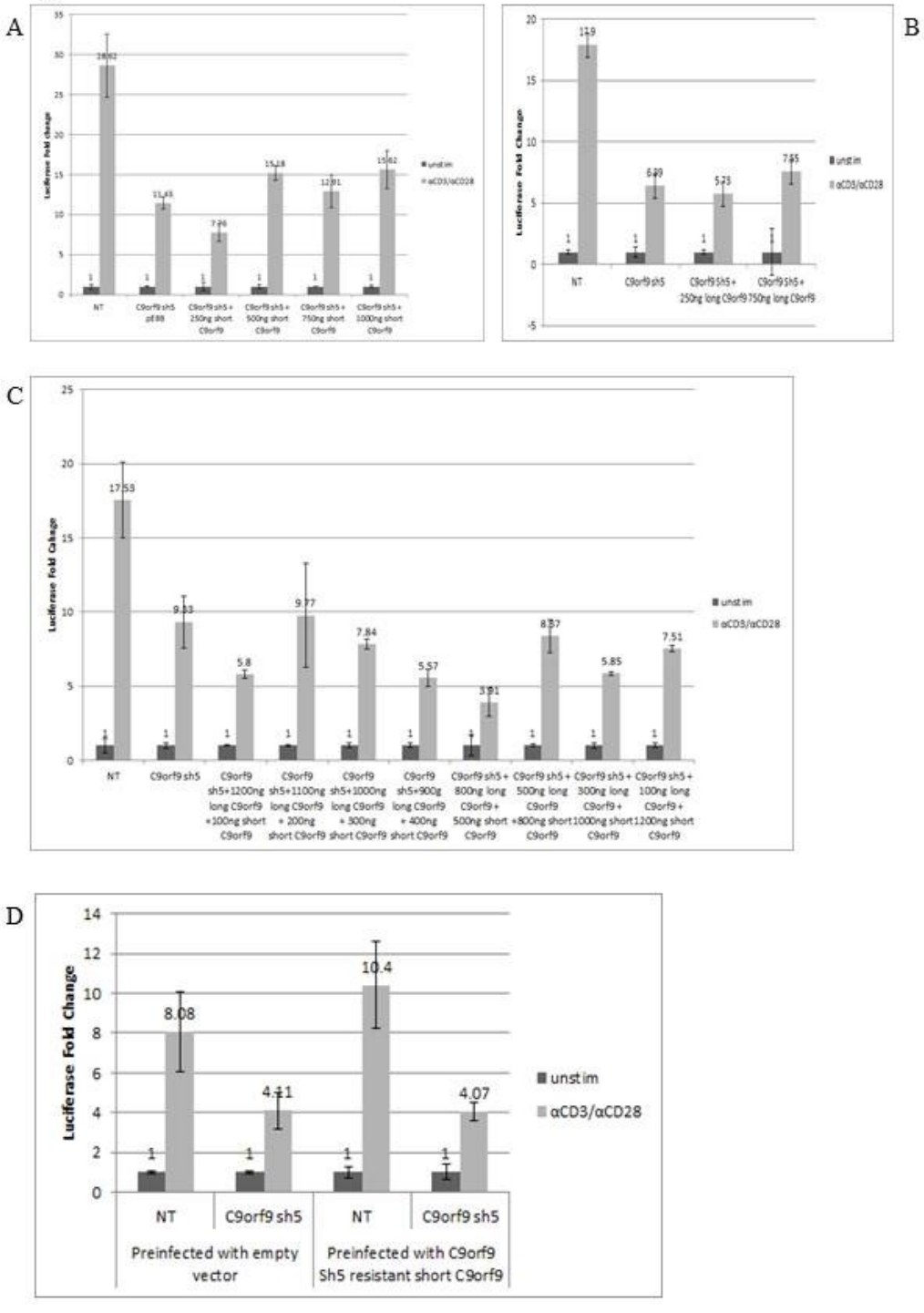
A
B
C
D
Luciferase Fold change
unstim
αCD3/αCD28
NT
C9orf9 sh5
C9orf9 sh5 + 250ng short C9orf9
C9orf9 sh5 + 500ng short C9orf9
C9orf9 sh5 + 750ng short C9orf9
C9orf9 sh5 + 1000ng short C9orf9
Luciferase Fold Change
C9orf9 sh5 + 250ng long C9orf9
C9orf9 sh5 + 750ng long C9orf9
C9orf9 sh5+1200ng long C9orf9 +100ng short C9orf9
C9orf9 sh5+1100ng long C9orf9 + 200ng short C9orf9
C9orf9 sh5+1000ng long C9orf9 + 300ng short C9orf9
C9orf9 sh5+900g long C9orf9 + 400ng short C9orf9
C9orf9 sh5 + 800ng long C9orf9 + 500ng short C9orf9
C9orf9 sh5 + 500ng long C9orf9 +800ng short C9orf9
C9orf9 sh5 + 300ng long C9orf9 + 1000ng short C9orf9
C9orf9 sh5 + 100ng long C9orf9 + 1200ng short C9orf9
8.08
4.11
10.4
4.07
Preinfected with empty vector
Preinfected with C9orf9 Sh5 resistant short C9orf9

Figure 7

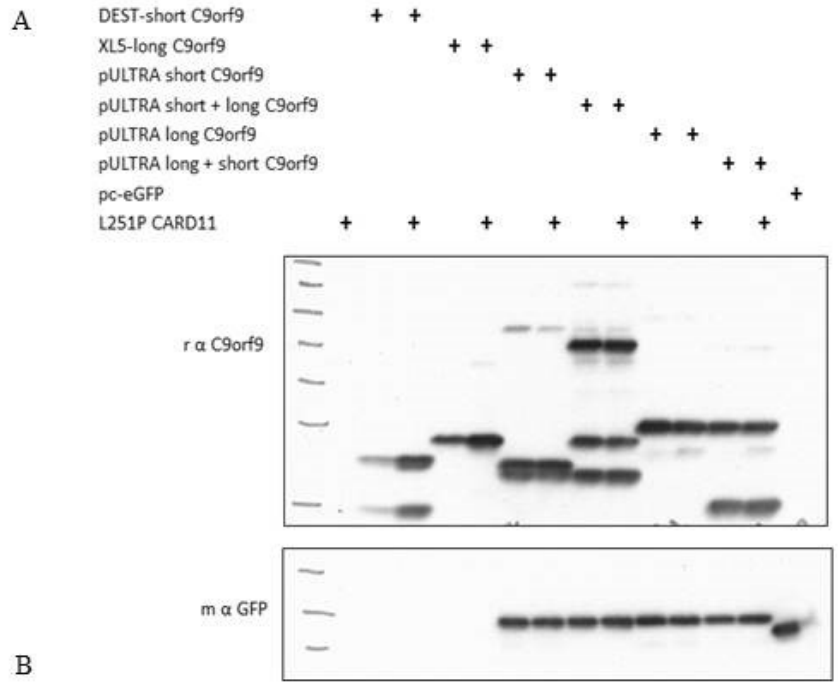
A
DEST-short C9orf9
XL5-long C9orf9
pULTRA short C9orf9
pULTRA short + long C9orf9
pULTRA long C9orf9
pULTRA long + short C9orf9
pc-eGFP
L251P CARD11
r α C9orf9
m α GFP

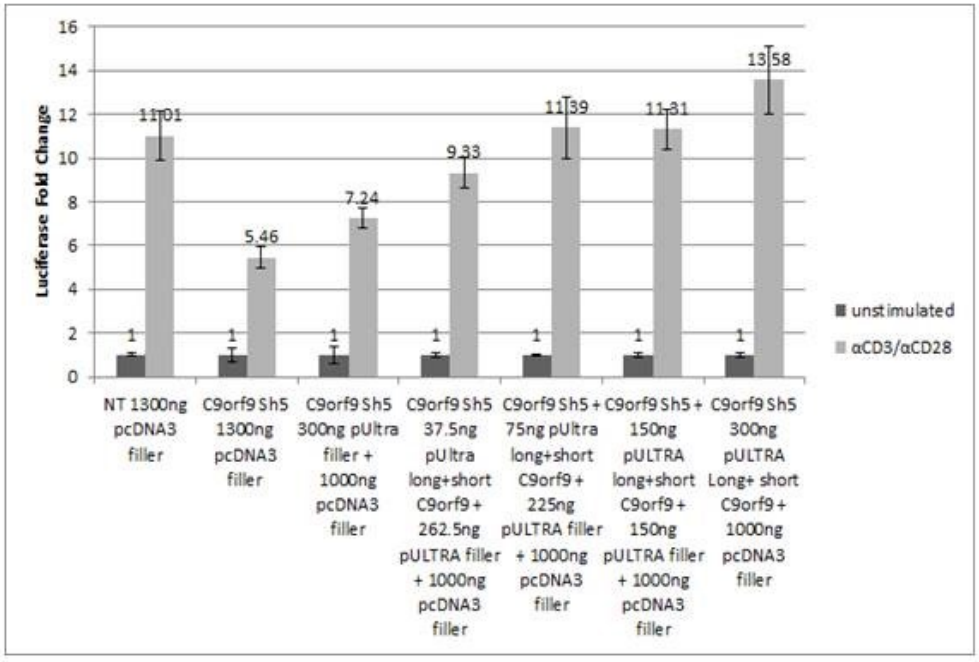
B
Luciferase Fold Change
16
14
12
10
8
6
4
2
0
11.01
5.46
7.24
9.33
11.39
11.31
13.58
1
unstimulated
αCD3/αCD28
NT 1300ng pcDNA3 filler
C9orf9 Sh5 1300ng pcDNA3 filler
C9orf9 Sh5 300ng pUltra filler + 1000ng pcDNA3 filler
C9orf9 Sh5 37.5ng pUltra long+short C9orf9 + 262.5ng pULTRA filler + 1000ng pcDNA3 filler
C9orf9 Sh5 + 75ng pUltra long+short C9orf9 + 225ng pULTRA filler + 1000ng pcDNA3 filler
C9orf9 Sh5 + 150ng pULTRA long+short C9orf9 + 150ng pULTRA filler + 1000ng pcDNA3 filler
C9orf9 Sh5 300ng pULTRA Long+ short C9orf9 + 1000ng pcDNA3 filler

Figure 8

A

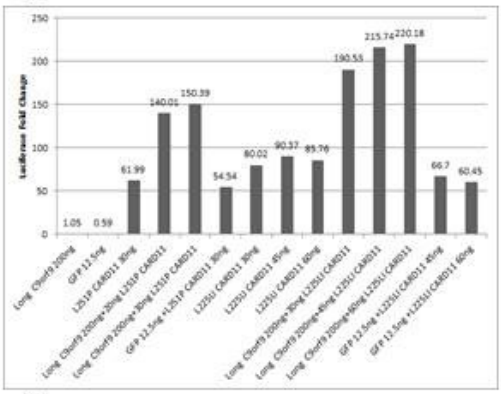
Luciferase Fold Change
1.05
0.59
61.99
140.01
150.39
54.54
80.02
90.37
85.76
190.55
215.74
220.18
66.7
60.45

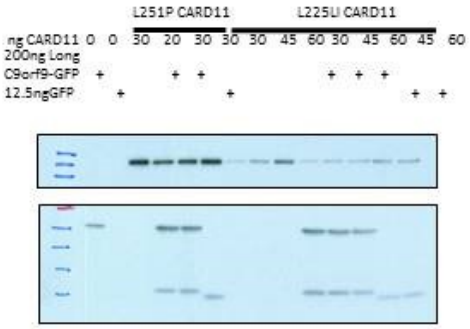
L251P CARD11
L225LI CARD11
ng CARD11 0 0 30 20 30 30 30 45 60 30 45 60 45 60
200ng Long C9orf9-GFP
12.5ngGFP

B

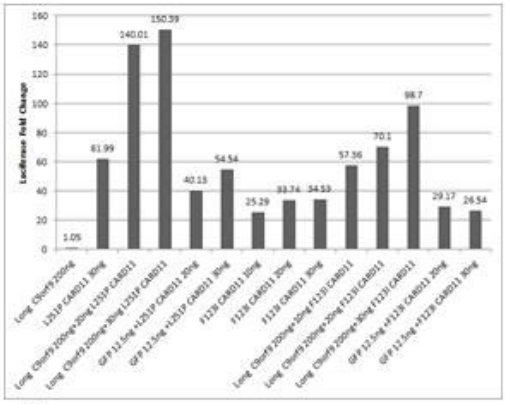
Luciferase Fold Change
1.05
61.99
140.01
150.39
40.13
54.54
25.29
33.74
34.53
57.36
70.1
98.7
29.17
26.54

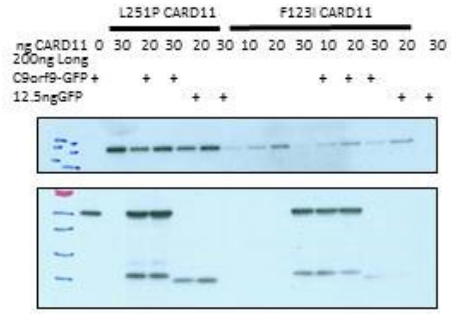
L251P CARD11
F123I CARD11
ng CARD11 0 30 20 30 20 30 10 20 30 10 20 30 20 30
200ng Long C9orf9-GFP
12.5ngGFP

C

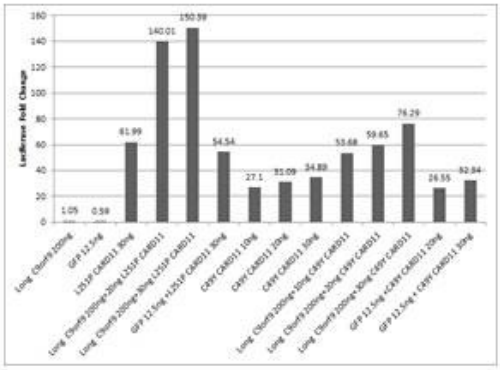
Luciferase Fold Change
1.05
0.59
61.99
140.01
150.39
54.54
27.1
31.09
34.89
53.68
59.65
76.29
26.55
32.94

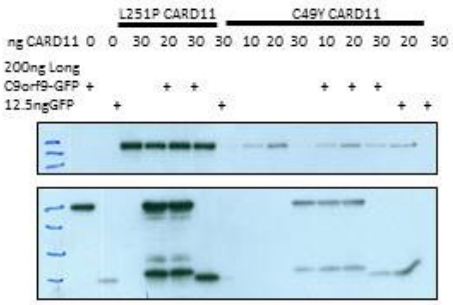
L251P CARD11
C49Y CARD11
ng CARD11 0 0 30 20 30 30 10 20 30 10 20 30 20 30
200ng Long C9orf9-GFP
12.5ngGFP

Figure 8 con't

D

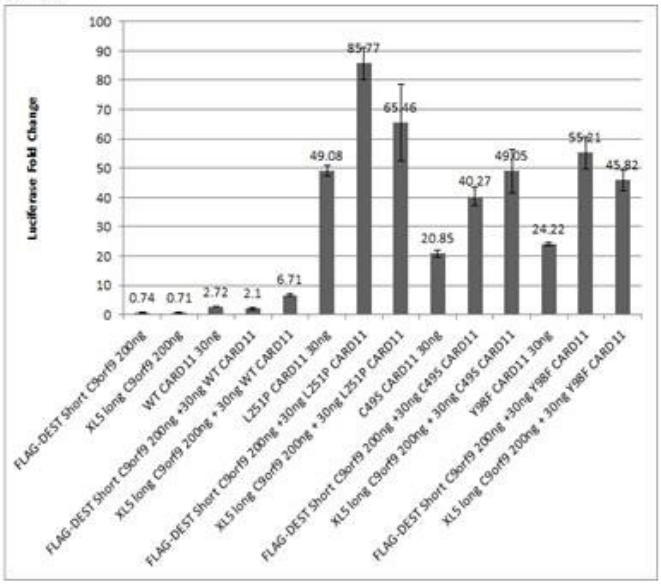

E

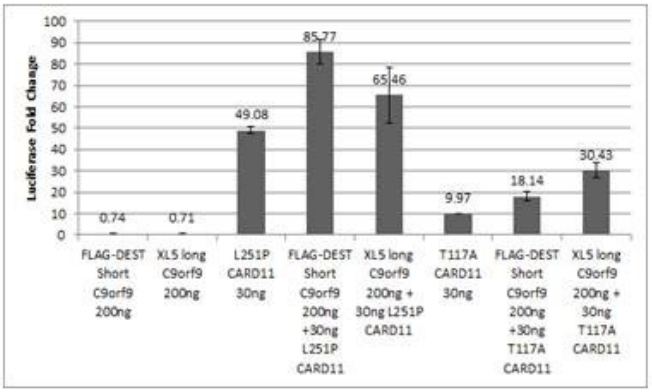

Figure 9

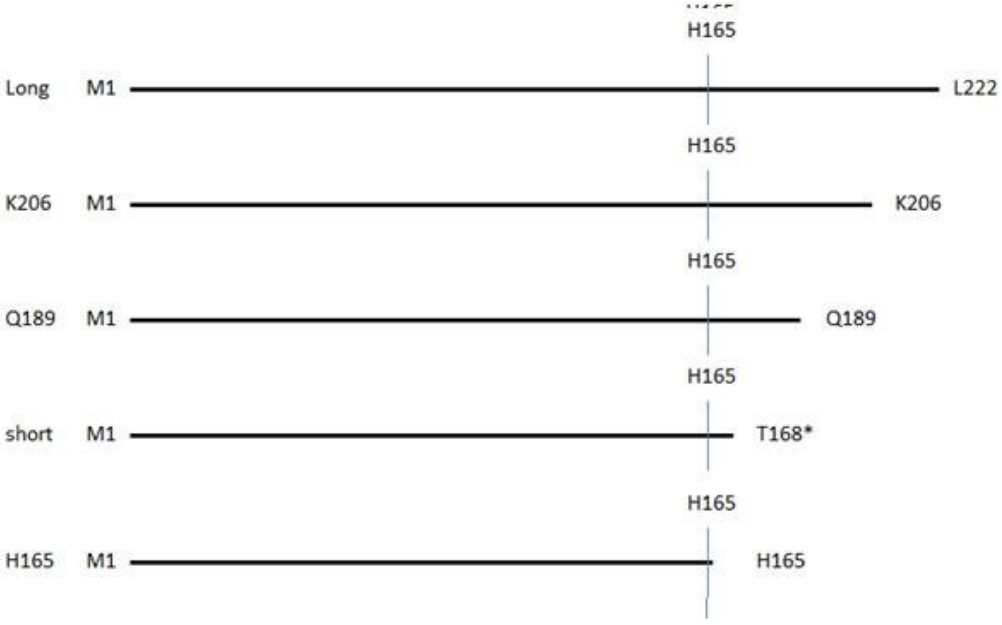
H165
Long M1 L222
H165
K206 M1 K206
H165
Q189 M1 Q189
H165
short M1 T168*
H165
H165 M1 H165

Figure 10

A

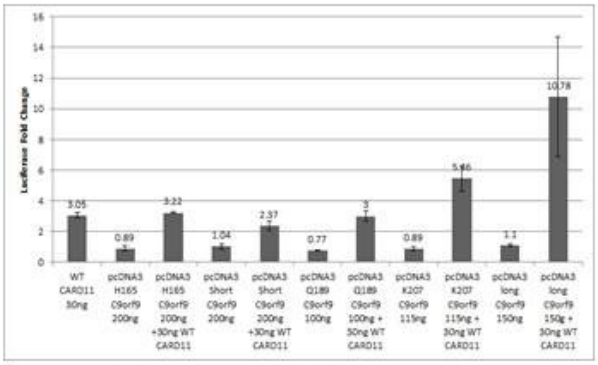
Luciferase Fold Change
16
14
12
10
8
6
4
2
0
3.05
0.89
3.22
1.04
2.37
0.77
3
0.89
5.46
1.1
10.78
WT CARD11 30ng
pcDNA3 H165 C9orf9 200ng
pcDNA3 H165 C9orf9 200ng +30ng WT CARD11
pcDNA3 Short C9orf9 200ng
pcDNA3 Short C9orf9 200ng +30ng WT CARD11
pcDNA3 Q189 C9orf9 100ng
pcDNA3 Q189 C9orf9 100ng + 30ng WT CARD11
pcDNA3 K207 C9orf9 115ng
pcDNA3 K207 C9orf9 115ng + 30ng WT CARD11
pcDNA3 long C9orf9 150ng
pcDNA3 long C9orf9 150g + 30ng WT CARD11

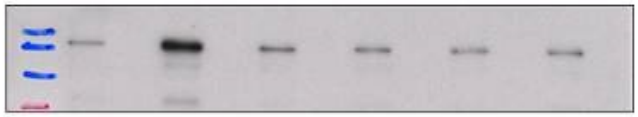
WB: m α myc (CARD11)

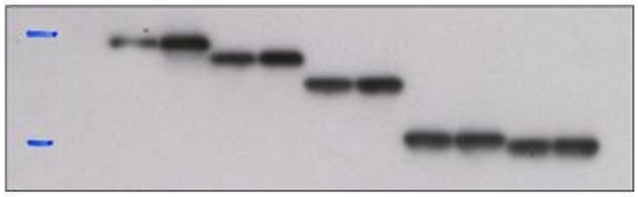
WB: r αC9orf9

B

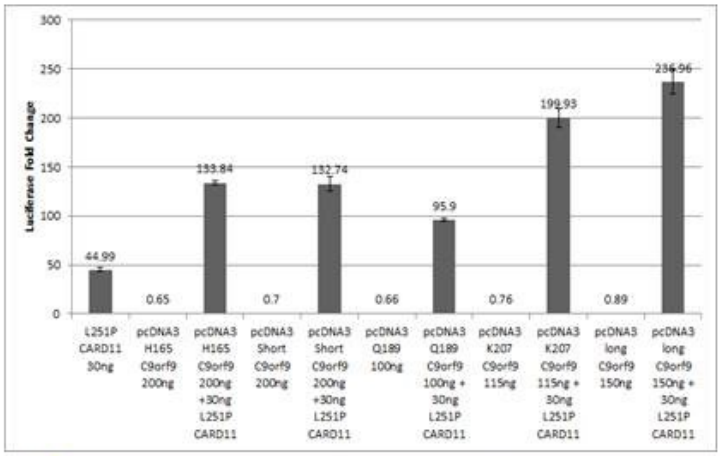
Luciferase Fold Change
300
250
200
150
100
50
0
44.99
0.65
133.84
0.7
132.74
0.66
95.9
0.76
199.93
0.89
236.96
L251P CARD11 30ng
pcDNA3 H165 C9orf9 200ng
pcDNA3 H165 C9orf9 200ng +30ng L251P CARD11
pcDNA3 Short C9orf9 200ng
pcDNA3 Short C9orf9 200ng +30ng L251P CARD11
pcDNA3 Q189 100ng
pcDNA3 Q189 C9orf9 100ng + 30ng L251P CARD11
pcDNA3 K207 C9orf9 115ng
pcDNA3 K207 C9orf9 115ng + 30ng L251P CARD11
pcDNA3 long C9orf9 150ng
pcDNA3 long C9orf9 150ng + 30ng L251P CARD11


WB: m α myc (CARD11)

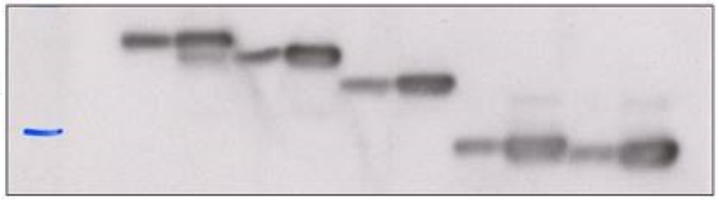
WB: r αC9orf9

Figure 11

A

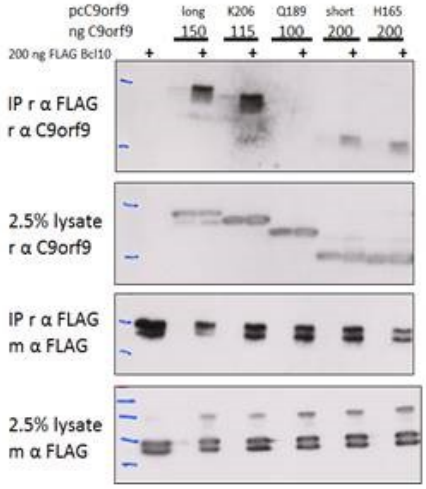

B

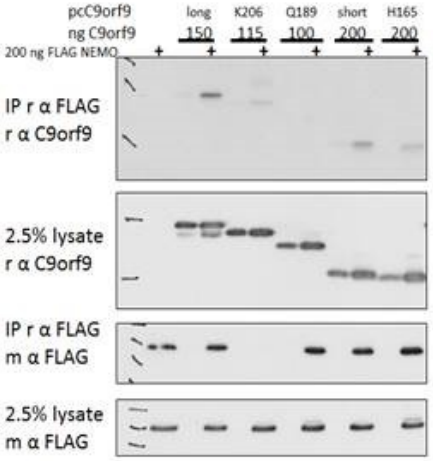

C

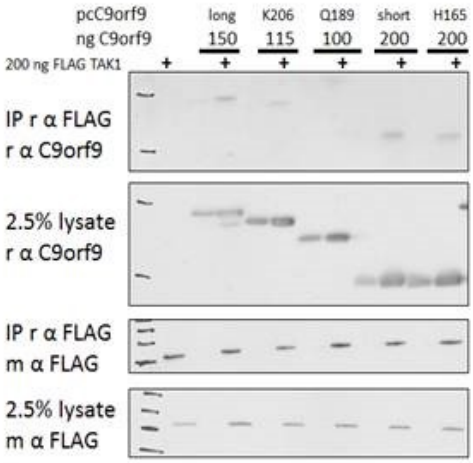

Figure 12

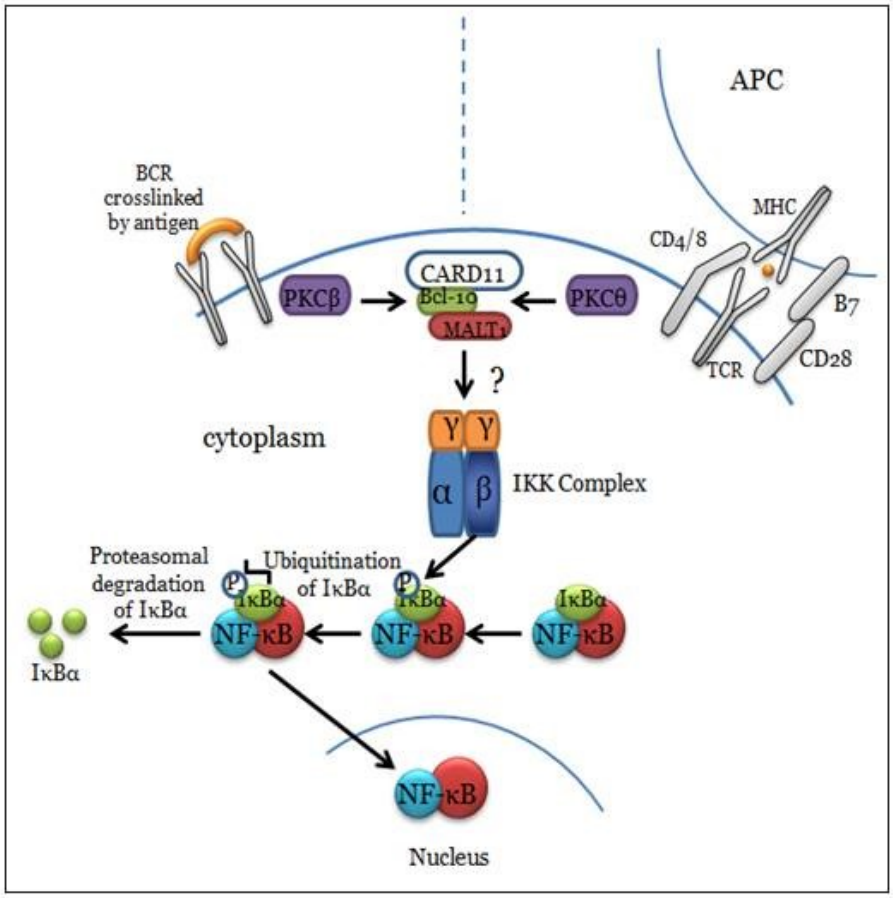
APC
BCR
crosslinked
by antigen
MHC
CD4/8
CARD11
Bcl-10
MALT1
PKCβ
PKCθ
B7
CD28
TCR
?
cytoplasm
γ γ
α β
IKK Complex
Proteasomal
degradation
of IκBα
Ubiquitination
of IκBα
P
IκBα
NF-κB
IκBα
Nucleus

Figure 13

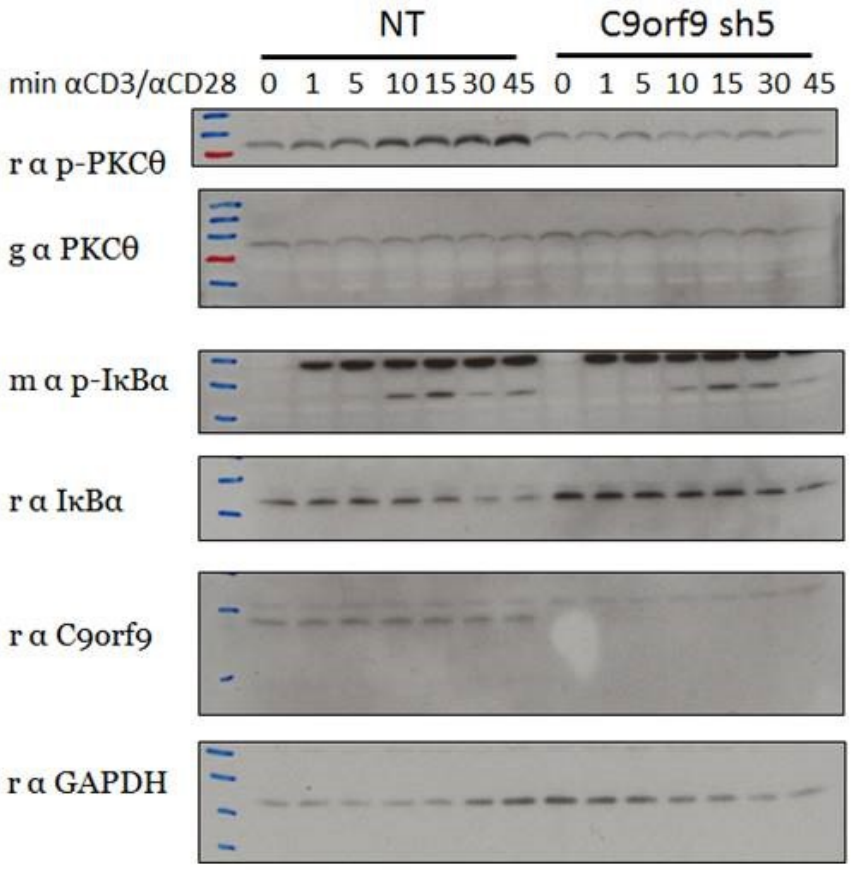
NT
C9orf9 sh5
min αCD3/αCD28 0 1 5 10 15 30 45 0 1 5 10 15 30 45
r α p-PKCθ
g α PKCθ
m α p-IκBα
r α IκBα
r α C9orf9
r α GAPDH

Figure 14

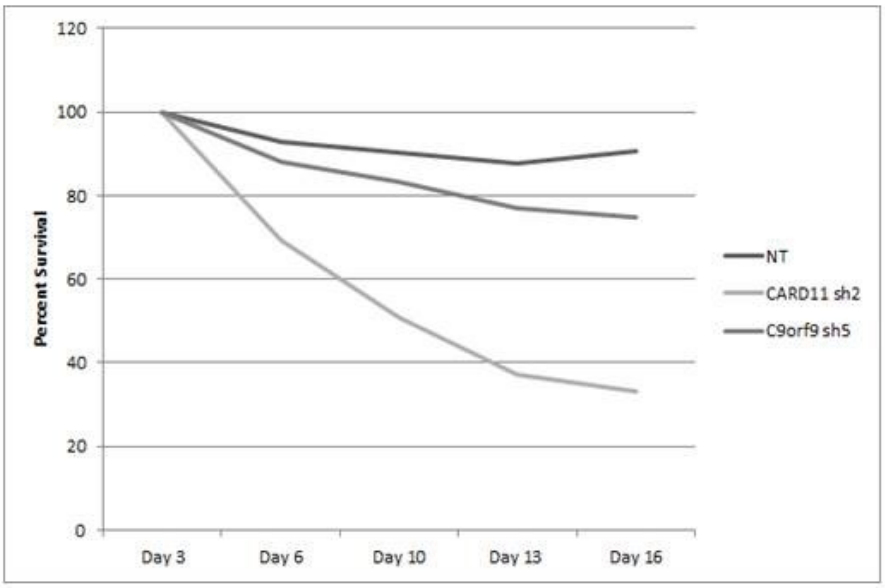
120
100
80
60
40
20
0
Percent Survival
Day 3
Day 6
Day 10
Day 13
Day 16
NT
CARD11 sh2
C9orf9 sh5

Figure 15

A

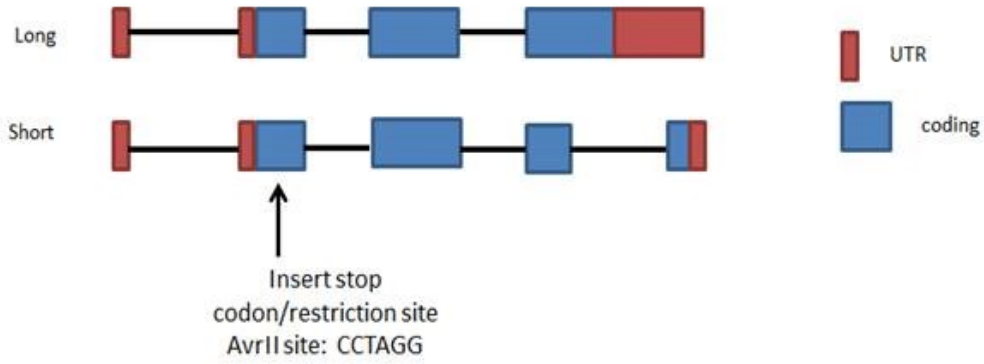

B

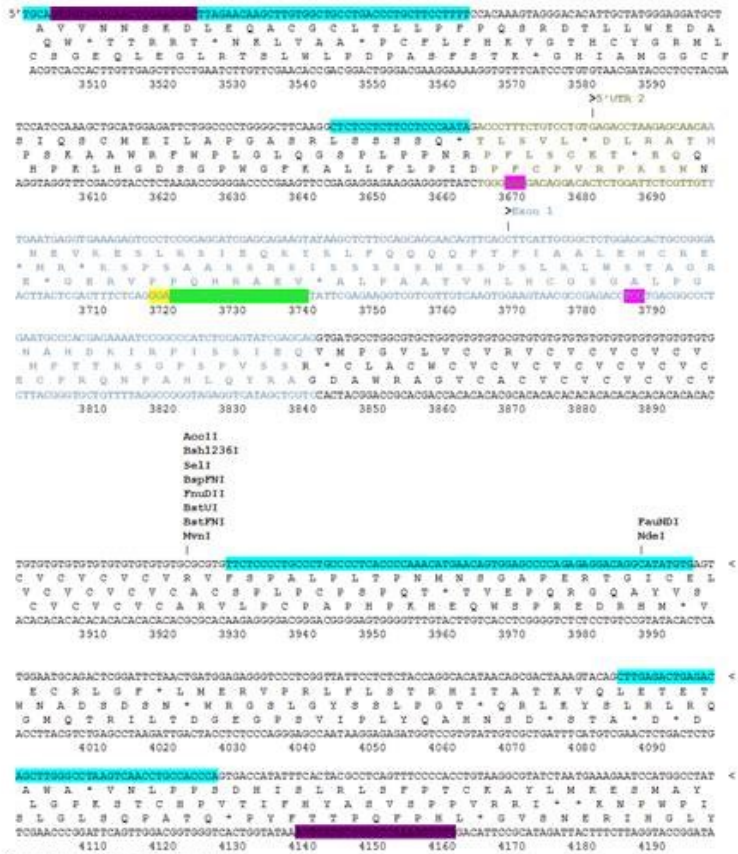

Green= proto spacer – actual targets
Yellow = PAM (including present but unused)
Blue= conserved intron
pink = boundaries of long oligo for HDR
Purple= genotyping primers

Figure 16

A

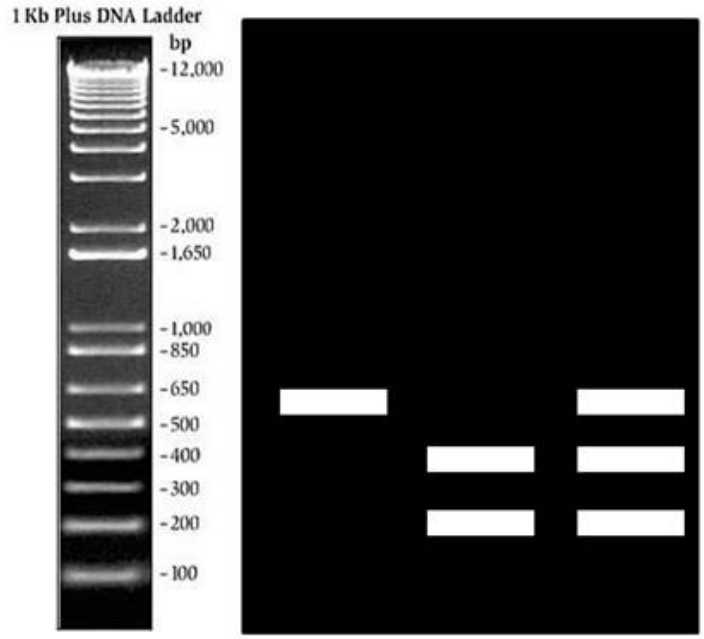
1 Kb Plus DNA Ladder
bp
12,000
5,000
2,000
1,650
1,000
850
650
500
400
300
200
100
0.9 µg/lane
Endogenous/no stop codon (Wild type)
640pb expected band
Stop codon insertion/ digest with AvrII Expected 414bp and 228bp (homozygous)
One endogenous allele and one modified allele (heterozygote)

B

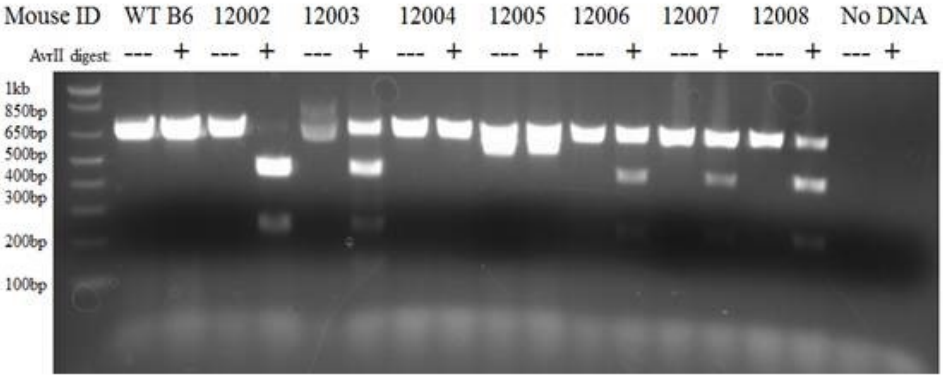
Mouse ID
WT B6
12002
12003
12004
12005
12006
12007
12008
No DNA
AvrII digest: --- + --- + --- + --- + --- + --- + --- + --- + --- +
1kb
850bp
650bp
500bp
400bp
300bp
200bp
100bp

Figure 17

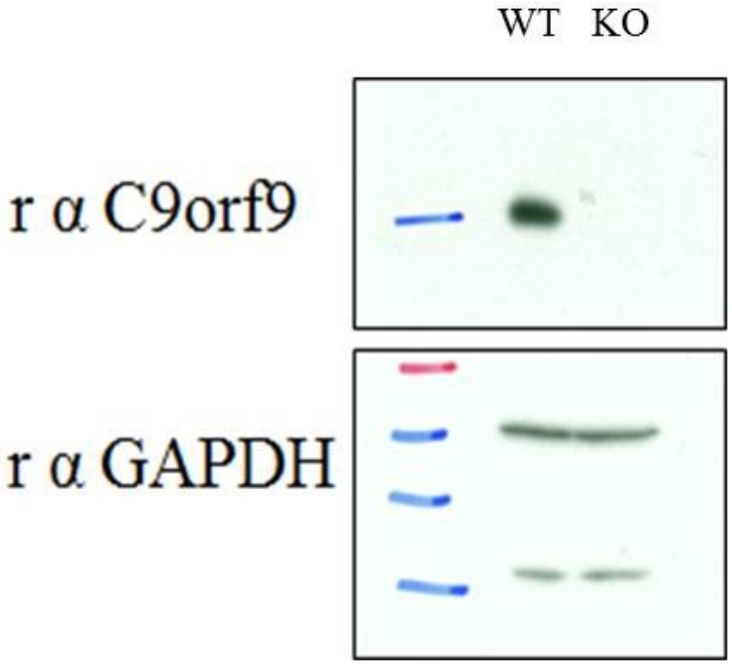

Figure 18

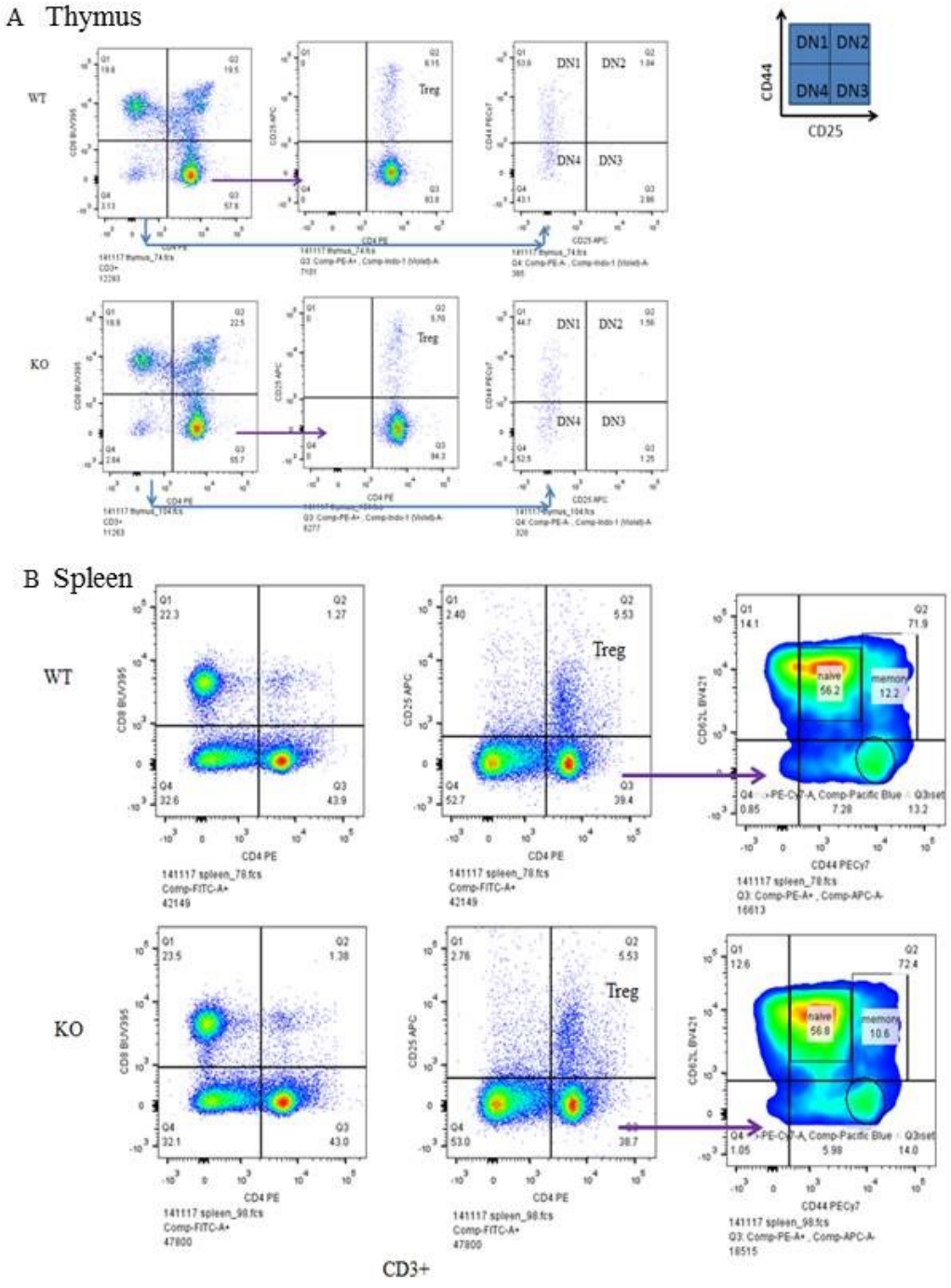
A Thymus
WT
KO
DN1
DN2
DN3
DN4
CD44
CD25
Treg
B Spleen
WT
KO
naive
memory
CD3+

Figure 19

A

	Pre-ProB	ProB	PreB	Immature B
B220	+	+	+	+
CD19	-	+	+	+
CD43	+	+	-	-
IgM	-	-	-	+

B Bone marrow

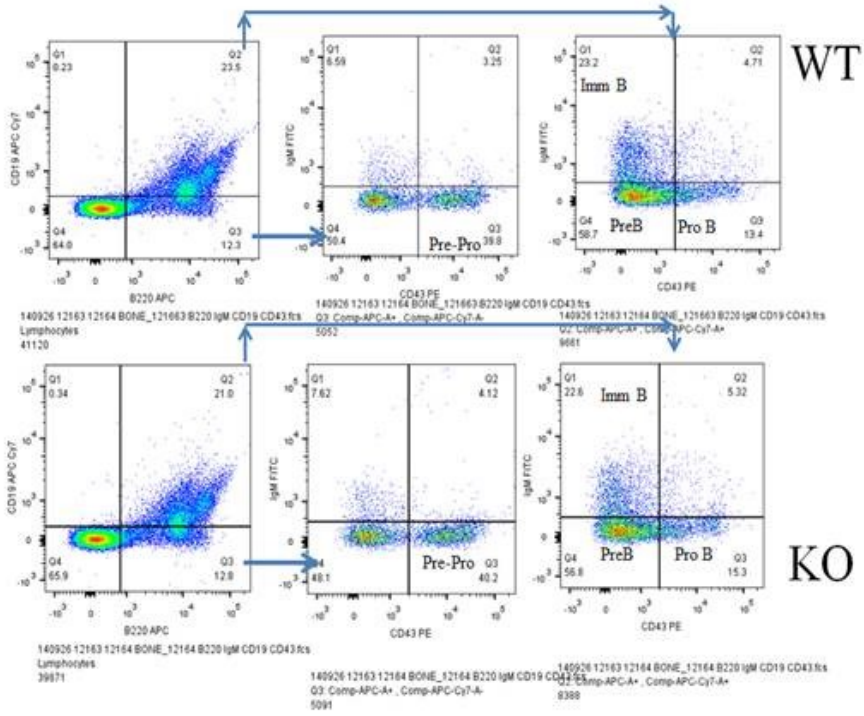

Figure 20
Splenic B cells

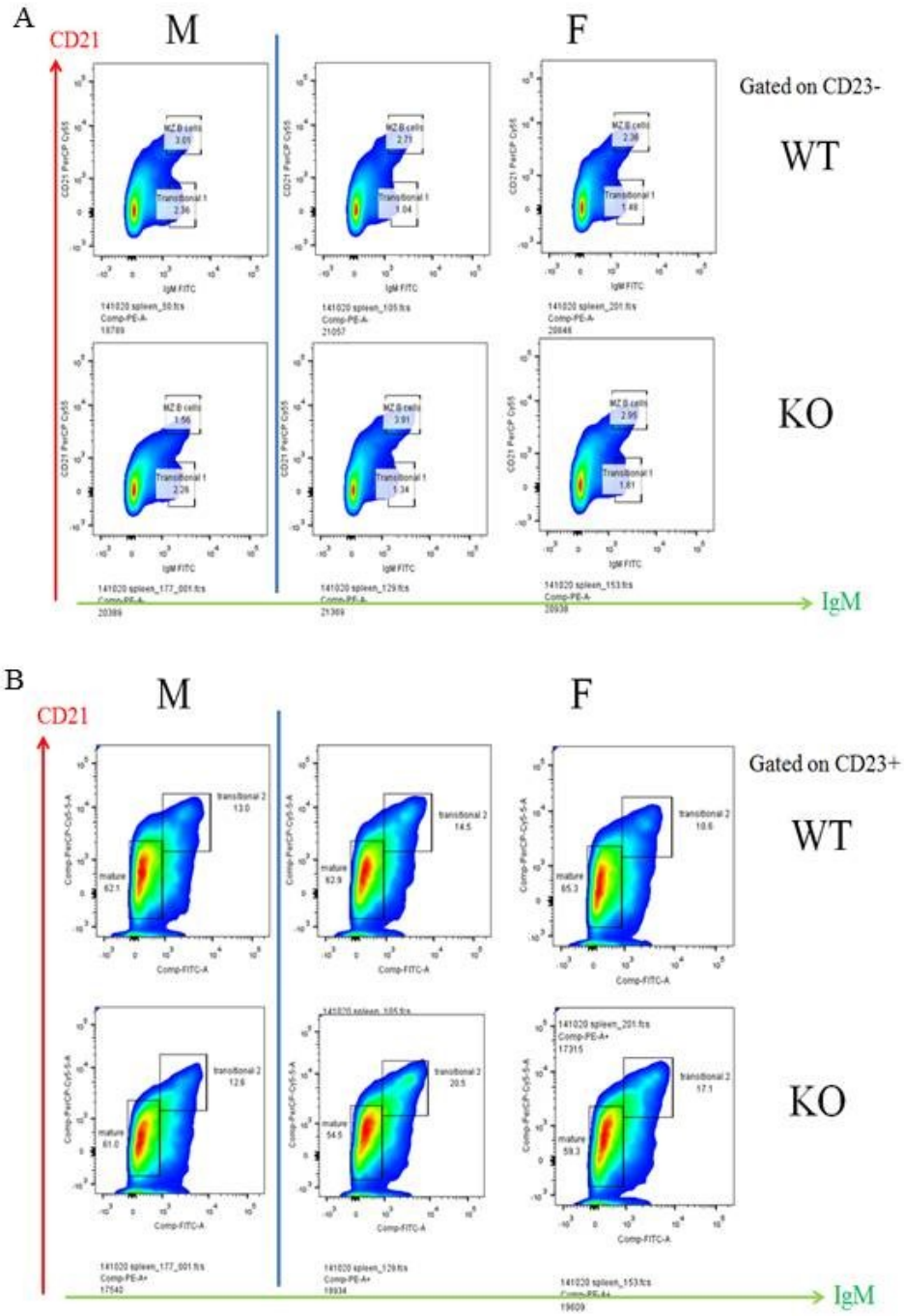

Figure 21

A

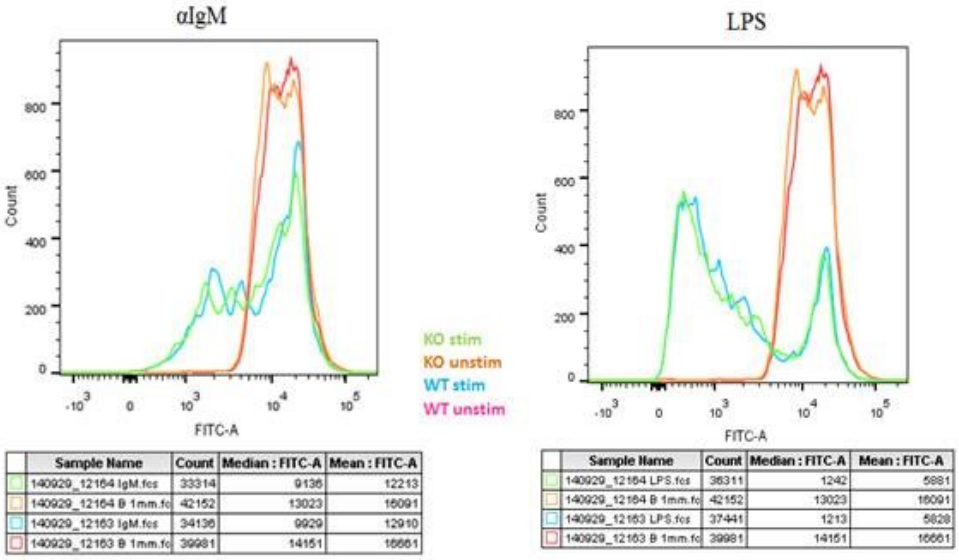

	Sample Name	Count	Median : FITC-A	Mean : FITC-A
	140929_12164 IgM.fcs	33314	9136	12213
	140929_12164 B 1mm.fc	42152	13023	16091
	140929_12163 IgM.fcs	34136	9929	12910
	140929_12163 B 1mm.fc	39981	14151	16661

	Sample Name	Count	Median : FITC-A	Mean : FITC-A
	140929_12164 LPS.fcs	36311	1242	5881
	140929_12164 B 1mm.fc	42152	13023	16091
	140929_12163 LPS.fcs	37441	1213	5828
	140929_12163 B 1mm.fc	39981	14151	16661

B

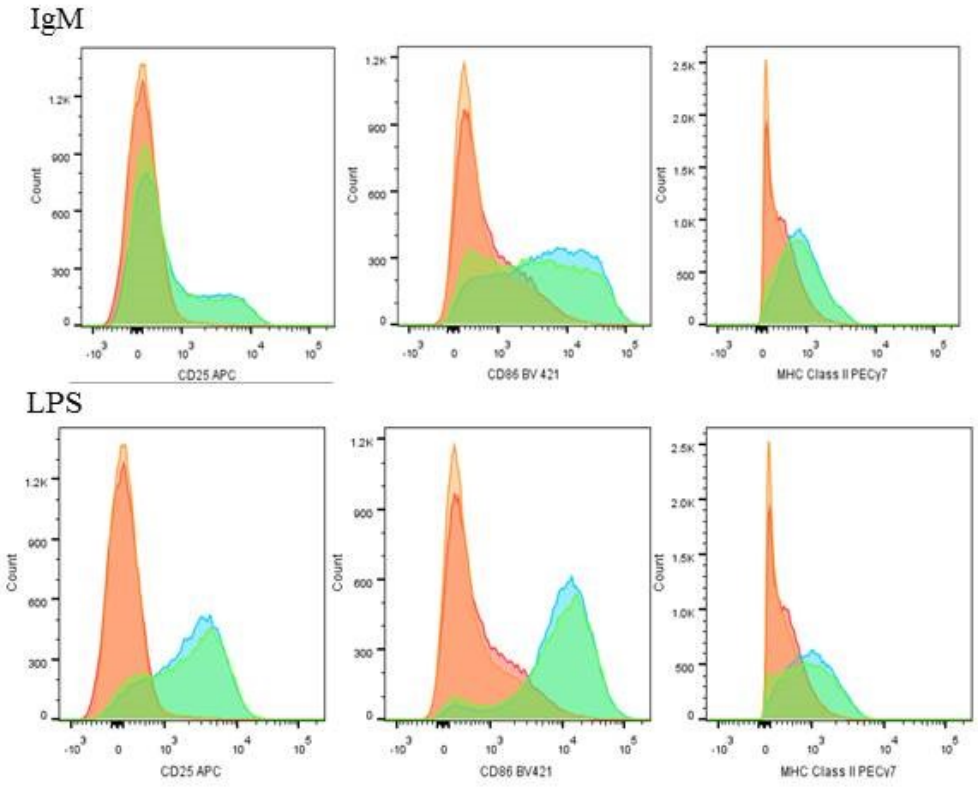

Figure 22

A

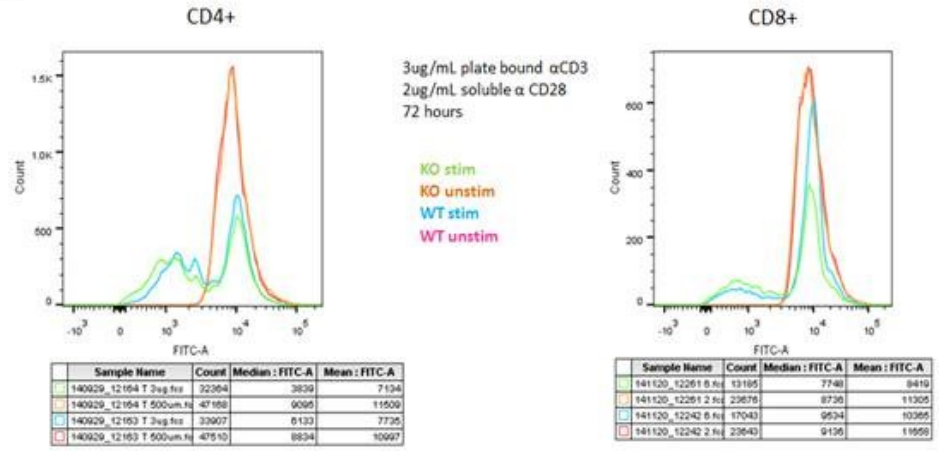

Sample Name	Count	Median : FITC-A	Mean : FITC-A
140929_12164 T 3ug.fcs	32364	3839	7134
140929_12164 T 500um.fc	47168	9095	11509
140929_12163 T 3ug.fcs	33907	6133	7735
140929_12163 T 500um.fc	47510	8834	10997

Sample Name	Count	Median : FITC-A	Mean : FITC-A
141120_12261 6.fcs	13185	7748	9419
141120_12261 2.fcs	23676	8736	11305
141120_12242 6.fcs	17043	9524	10365
141120_12242 2.fcs	23643	9136	11668

B

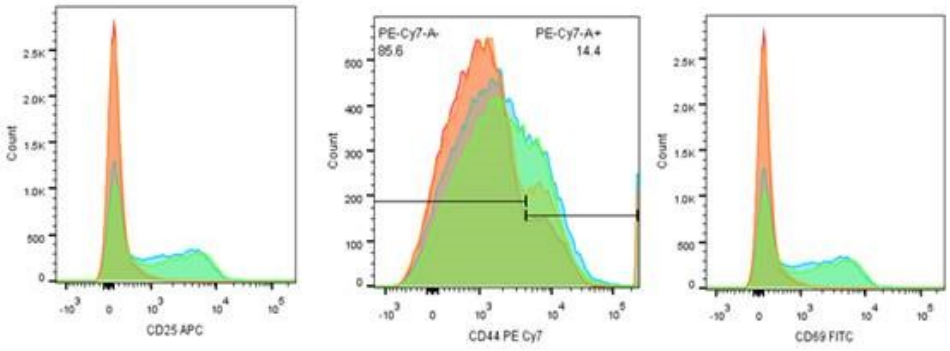

Figure Legends

Figure 1: Structure of CARD11 and relevant gain of function mutations. Schematic diagram of the domains of CARD11, including the CARD, LATCH, Coiled Coil, Inhibitory, PDZ, SH3, and GUK domains. Relevant gain-of-function mutations in the CARD, LATCH, and Coiled Coil domains are indicated.

Figure 2: Activation of NF-κB in 293Ts by short C9orf9 and CARD11. HEK293T cells were transfected with 20ng Igκ$_2$-IFN-luc, 6ng pCSK-LacZ and the indicated amounts of DEST-V5-short C9orf9 and/or the indicated amounts of pc-Myc-CARD11.

Figure 3: C9orf9 has a specific effect on TCR-to-NF-κB signaling in Jurkat T cells. **A**. Jurkat T cells were transfected with 1500ng Igκ$_2$-IFN-luc, 200ng pCSK-LacZ, and 1300ng pcDNA3 and stimulated for 5 hours with anti-CD3/anti-CD28. Jurkat T cells were transfected with 1500ng NFAT-luc, 200ng pCSK-LacZ, and 1300ng pcDNA3 and stimulated for 5 hours with anti-CD3/anti-CD28. **C**. Jurkat T cells were transfected with 1500ng Igκ$_2$-IFN-luc, 200ng pCSK-LacZ, and 1300ng pcDNA3 and stimulated for 5 hours with anti-CD3/anti-CD28 or TNF.

Figure 4: Western blot of C9orf9 knockdown Jurkat lysates indicates two isoforms of C9orf9. Western blot analysis of lysates from C9orf9 knockdown or control Jurkat T cells. A blot for IKKα is shown as a loading control.

Figure 5: Structure of C9orf9 locus and locations of shRNA targeting. A. A schematic diagram of the chromosomal locus of C9orf9 indicating the locations of the UTRs and coding regions and showing the relative positioning of these with regards to the short and long isoforms. **B**. A diagram of the long mRNA transcript of C9orf9. The

coding region is translated and the targets of three shRNA hairpins are highlighted. **C.** Jurkat T cells were were transfected with 1500ng Igκ$_2$-IFN-luc, 200ng pCSK-LacZ, and 1300ng pcDNA3 and stimulated for 5 hours with anti-CD3/anti-CD28.

Figure 6: Single isoform rescue of C9orf9 knockdown Jurkats is unsuccessful. Jurkat T cells were transfected with 1500ng Igκ$_2$-IFN-luc, 200ng pCSK-LacZ, and stimulated for 5 hours with anti-CD3/anti-CD28. In all panels, NT indicates cells infected with a non-target shRNA, while C9orf9 sh5 indicates that cells were infected with an shRNA targeting C9orf9. **A.** Cells were also transfected with the indicated nanogram amounts of pEBB short sh5-resistant C9orf9. **B**. Cells were also transfected with the indicated nanogram amounts of pEBB long sh5-resistant C9orf9. **C**. Cells were transfected with the indicated nanogram amounts of pcDNA3 sh5-resistant short C9orf9 and pCMV-XL5 sh5-resistant long C9orf9. **D.** Cells were pre-infected with empty pCLIN3A or pCLIN3A sh5-resistant short C9orf9 before infection with the relevant shRNA.

Figure 7: Pseudo-polycistronic vector expresses two isoforms of C9orf9 and successfully rescues C9orf9 knockdown phenotype in Jurkat T cells. A. Western blot analysis of HEK293T cells transfected with pcDEST-V5 short C9orf9, pCMV XL5 long C9orf9, pULTRA short C9orf9, pULTRA short + long C9orf9, pULTRA long C9orf9, pULTRA long + short C9orf9, or pc-eGFP in the presence or absence of pc-myc L251P CARD11. **B.** Jurkat T cells were transfected with with 1500ng Igκ$_2$-IFN-luc, 200ng pCSK-LacZ, 1000ng pcDNA3, and 300ng total of pULTRA long + short sh5-resistant

C9orf9 and empty pULTRA as indicated and stimulated for 5 hours with anti-CD3/anti-CD28

Figure 8: C9orf9 enhances the ability of hyperactive CARD11 and Bcl10 to signal to NF-κB. HEK293T cells were transfected with 20ng Igκ$_2$-IFN-luc, 6ng pCSK-LacZ and the indicated amounts of pc long C9orf9-GFP or 12.5ng of pc-EGFP in the presence or absence of the indicated nanogram amounts of pc-Myc-CARD11 L251P and **A.** L225LI CARD11 **B.** F123I CARD11 or **C.** C49Y CARD11. **D.** Y98F CARD11 **E.** T117A CARD11 **F.** HEK29T cells were transfected with 20ng Igκ$_2$-IFN-luc, 6ng pCSK-LacZ and 200ng DEST-FLAG short C9orf9, pCMV XL5 long C9orf9, 30ng pc FLAG-Bcl10, or a combination of C9orf9 and Bcl10. Panels A, B, and C include Western blot analysis of lysates from these transfections.

Figure 9: Structure of C9orf9 truncation constructs. Schematic of C9orf9 truncation constructs. For each construct, the starting methionine is labeled M1 while the terminating residue is indicated on the right of the diagram. For each construct H165 is marked as the splice site where the short and long isoforms diverge. T168 is labeled with (*) in short C9orf9 to indicate that the three resides after H165 are different in this construct than in the Long, K206, and Q189 constructs.

Figure 10: C9orf9 truncation constructs have different effects on CARD11 signaling. . HEK293T cells were transfected with 20ng Igκ$_2$-IFN-luc, 6ng pCSK-LacZ and the indicated amounts of the appropriate pcC9orf9-GFP constructs in the presence or absence of **A.** 30ng pc-Myc-CARD11 or **B.** 30ng L251P CARD11. Western blot analysis of lysates from these transfections is included in both panels.

Figure 11: C9orf9 truncation constructs interact with CARD11 cofactors. HEK293T cells were transfected with the indicated nanogram amounts of the appropriate pcC9orf9 construct and 200 ng of **A.** pcFLAG-Bcl10 **B.** pcFLAG-NEMO **C.** CMV FLAG mTAK1. Anti-FLAG IPs were performed and the results were analysed by anti-C9orf9 and anti-FLAG Western blots.

Figure 12: Schematic diagram of CARD11's role in antigen receptor signaling. Schematic diagram of the TCR-to-NF-κB and BCR-to-NF-κB pathways indication their convergence on CARD11.

Figure 13: Activation of TCR pathway proteins is affected by C9orf9 knockdown in Jurkat T cells. Jurkat T cells were stimulated with anti CD3/antiCD28. Cells were lysed in the presence of protease inhibitor cocktail (Sigma P8340 at 1:1000), 10mM sodium fluoride, 2.5mM sodium orthovanadate, and 10mM β-glycerophosphate. Equal volume of lysate was run per lane on 12% SDS-PAGE and results were analyzed via Western blot.

Figure 14: C9orf9 knockdown does not affect OCI-Ly3 cell line survival. Retroviral constructs based on the pSUPER-retro-Neo+GFP vector containing either a non-target shRNA, a CARD11-targeting shRNA, or a C9orf9-targeting shRNA were packaged using pCL-Eco and used to infect the OCI-Ly3 DLBCL cell line. Three days after infection cells were analyzed by FACS and the percent GFP+ (indicating live cells infected with the shRNA vector) were calculated. This procedure was repeated at 6, 10, 13, and 16 days post infection.

Figure 15: C9orf9 locus and CRISPR targeting design. A. The schematic of the C9orf9 locus which indicates the CRISPR sgRNA target site. **B.** The sequence of the second exon of C9orf9 and some of the surrounding introns. Regions of interested are indicated by highlighting: blue indicates conserved intron regions, pink indicates the extent of the 126bp oligo used for homology directed repair, yellow indicates the PAM, green indicates the protospacer sgRNA target, and purple indicates the locations of the sequencing primers used in genotyping pups.

Figure 16: PCR genotyping strategy of C9orf9 knockout mice. A. A schematic cartoon indicating the potential outcomes of WT, C9orf9 KO, and heterozygous pups in the described genotyping strategy. **B.** An image taken from the genotyping PCR of a control C57/B6 WT mouse and the first seven pups born after CRISPR genome editing of single-cell embryos. Each mouse has two lanes, a control lane and one where the sample was digested overnight with 0.5ul AvrII. Although 12002, 12006, 12007, and 12008 all appear to have at least one copy of the desired gene modification, it is important to note that only 12008 transmitted this allele to its offspring.

Figure 17: C9orf9 expression is decreased in C9orf9 knockout mice. Mouse testes from WT C57/B6 and C9orf9 KO mice were harvested, lysed, and protein was quantitated by Bradford assay. 20ug total protein was run per lane on 12% SDS-PAGE. Protein was transferred to PVDF and membranes probed for C9orf9 and GAPDH as a loading control.

Figure 18: T cell development in the thymus and spleen is normal in C9or9f knockout mice A. Mouse thymocytes were stained for T cell development and analyzed

by flow cytometry. Cells were gated on CD3+ and then stratified on CD4+ and CD8+. CD4+ cells were gated and stratified on CD25 to distinguish Treg cells from other effector cells. CD4-CD8- cells were stratified on CD25 and CD44 to look at the Double Negative 1-4 (DN1-4) developmental populations. **B.** Mouse splenocytes were stained for T cell development and analyzed by flow cytometry. Cells were gated on CD3+ and then stratified by CD4+ and CD8+. CD4+ cells were stratified on CD25 to distinguish Treg cells from other effector cells. CD4+CD25- cells were then stratified on CD44 and CD62L to compare naïve (CD44med CD62L+), memory (CD44hiCD62L+) and effector (CD44+CD62L-) populations.

Figure 19: B cell development in the bone marrow of C9or9f knockout mice is normal. A. Chart comparing the expression of B220, CD19, CD43, and IgM in Pre-ProB cells, proB cells, preB cells, and immature B cells. **B.** Mouse bone marrow cells were stained for B cell development and analyzed by Flow Cytometry. Cells were stratified on B220 and CD19. B220+CD19- cells were stratified on CD43 and IgM to identify Pre-Pro B cells. B220+CD19+ cells were stratified on CD43 and IgM to identify Pro B, Pre B, and Immature B cells. Wild type mice are on the top row of the panel while C9orf9 KO mice are on the bottom row of the panel.

Figure 20: Splenic B cells show normal development in C9orf9 knockout mice. Mouse splenocytes were stained for B cell development and analyzed by flow cytometry. Males are in the far left column, while two female mince per genotype were analyzed in the center and right hand columns. Wild type mice are at the top of each panel and C9orf9 KO mice are on the bottom row of each panel. Cells were stratified on CD23. **A.**

CD23- cells were then stratified on CD21 and IgM to compare Marginal Zone B cells (MZB cells, IgMhiCD21hi) and Transitional 1 cells (IgMhiCD21lo). **B.** CD23+ cells were stratified on IgM and CD21 to compare Transitional 2 cells (IgMhiCD21hi) and mature cells (IgM-CD21lo).

Figure 21: B cell activation in C9orf9 knockout mice is normal. Mouse B cells analyzed for activation after stimulation. In both panels, green demotes stimulated C9orf9 KO cells, orange denotes unstimulated C9orf9 KO cells, blue indicates stimulated wild type cells and pink represents unstimulated wild type cells. **A.** Cells were loaded with CFSE (final concentration 2μM) and stimulated with 10μg/mL anti-IgM or 20ug/mL LPS. After 72 hours cells were harvested and analyzed for division by flow cytometry. **B.** Cells were stimulated overnight with anti-IgM or LPS. Cells were then harvested and stained for the activation markers CD25, CD86, and MHC Class II and analyzed by flow cytometry.

Figure 22: T cell activation in C9orf9 knockout mice is normal. Mouse T cells were analyzed for activation after stimulation. In both panels, green demotes stimulated C9orf9 KO cells, orange denotes unstimulated C9orf9 KO cells, blue indicates stimulated wild type cells and pink represents unstimulated wild type cells. All stimulations were performed with 3μg/mL plate bound αCD3 and 2 μg/mL soluble αCD28. **A.** CD4+ (left panel) and CD8+ (right panel) cells were loaded with CFSE (Final concentration 1μM) and incubated for 72 hours in the presence or absence of stimulation. Cells were harvested and analyzed for division by flow cytometry. **B.** CD4+ cells were incubated

overnight in the presence or absence of stimulation. Cells were harvested and stained for the activation markers CD25, CD44, and CD69 and analyzed by flow cytometry.

Experimental Methods:

Reporter assays of 293T cells:

HEK293T cells were grown in Dulbecco's modified Eagle's medium supplemented with 10% heat inactivated fetal bovine serum, 2mM glutamine, and 100 U/ml each of streptomycin and penicillin. Cells were maintained at 37°C in humidified atmosphere with 5% CO_2. For transfection, 0.5mL cells were plated at $1.8x10^5$/mL in 24 well plates. 24 hours after plating, cells were transfected using the calcium phosphate method. Briefly, 376ng total DNA were transfected, including 20ng of the IgK_2-IFN-Luc reporter plasmid [38] or the NFAT-Luc reporter plasmid (Stratagene) [9], 6ng of the pCSK-LacZ plasmid [3], and up to 350ng of the expression constructed to be tested. Each sample was transfected with pcDNA3 filler DNA to maintain the 376ng total. Media was changed between 20-26 hours after transfection, and cells were harvested between 44-48 hours after transfection. Harvest was performed by lysing cells in 100ul 1x reporter lysis buffer (Promega). Cells were scraped and spun at 16,000 x *g* for 5 minutes to pellet cells. 20ul of lysate were used to measure luciferase activity using the Promega luciferase reporter system and read on a Berthold TriStar LB941 luminometer. β-Galactosidase (β-Gal) activity was measured using 10ul lysate, 15ul 1x Promega lysis buffer, and using a chemiluminescent reporter system (Roche) according to the manufacturer's instructions. Relative signaling activity was determined by subtracting the background signal as measured in untransfected cells, dividing the luciferase activity by the β-Gal activity, and normalizing to a reference sample transfected with 350ng of empty expression vector.

Jurkat reporter assays:

Jurkat T cells were grown in RPMI media supplemented with 10% heat-inactivated fetal bovine serum, 2mM glutamine, 100 U/mL each of streptomycin and penicillin, and 50μM β-mercaptoethanol. Cells were maintained at 37°C in humidified atmosphere with 5% CO_2. On the day of transfection, $5x10^5$ cells were plated in 2mL of media in 6-well plates. In all assays, cells were transfected with 1500ng of either IgK_2-IFN-Luc or NFAT-LUC, 200ng of pCSK-LacZ, and 1300ng of expression and/or filler DNA, for a total of 3ug. DNA was incubated with 9ul of LT-1 (Mirrus) transfection reagent in the presence of serum-free RPMI before being added dropwise to cells. 40-44 hours after transfection, cells were resuspended in 1mL of medium with or without 1μg/mL each of anti-human CD3 (BD clone UCHT1), anti-human CD28 (BD), and anti-mouse IgG1 (BD). Alternatively, cells were resuspended in 1mL media containing 10ng/mL TNF (Sigma). Cells were incubated 4-6 hours, and were then harvested and lysed in 150μL 1x Promega lysis buffer. Cells were spun as above to remove debris. Luciferase activity was measured using 50μL lysate, while β-Gal activity was measured using 25μL lysate and the reporter system described above.

HEK293T Immunoprecipitation

Cells were transfected using the calcium phosphate method described above, except that cells were $5x10^5$ cells were plated in 2mL media in 6 well plates. A total of 2μg DNA was transfected 20-24 hours after plating. Media was changed 20-24 hours after transfection, and cells were harvested 44-48 hours after transfection. Cells were

harvested in ice and lysed in 500µL IP Lysis buffer containing 150mM NaCl, 1mM EDTA, 10% glycerol, 1% IGEPAL, 50mM HEPES pH 7.9, and a protease inhibitor cocktail (Sigma P8340). Cells were spun for 10min at 16,000 x *g* at 4°C to remove debris. 450µl lysate were transferred to a new tube for preclearing. Lysates were precleared once for 30 minutes with rotation at 4°C using a 7ul bed volume of Protein G Sepharose 4 Fast Flow (GE). 10µL of precleared lysate was saved for Western Blotting. Immunoprecipitation was achieved by incubating 40µl precleared lysate with 1µg rabbit anti-Flag antibody (Sigma F7425) overnight at 4°C with rotation. A 7µl bed volume of protein G Sepharose that had been blocked overnight in 1% insulin was added to each sample and rotation continued at 4°C for one hour. After this incubation, the beads were washed four times with 1mL IP Lysis Buffer for 5 minutes with rotation at 4°C. After the final wash, the resulting complex was eluted from the bead/antibody complex using 30µl 0.1mg/mL FLAG peptide (Sigma). Two thirty-minute elutions were performed and the elutions were pooled together and spun briefly. 30µL of the resulting eluate was boiled with presence of 15µL 3X sodium dodecyl sulfate-polyacrylamide gel electrophoresis (SDS-PAGE) loading buffer (150mM Tris-HcL pH6.8, 6% SDS, 0.3% Bromophenol blue, 30% glycerol, 15% β-mercaptoethanol) and resolved on 12% SDS-PAGE gels. Samples were transferred to polyvinylidene difluoride (PVDF) membranes and blotted for C9orf9 (Sigma HPA022243 or Abcam 171036) and FLAG (Sigma F1804).

Stable knockdown and Rescue of C9orf9

A hairpin targeting C9orf9 (C9sh5, target sequence 5'-AGAGCTACATGGAACACTACT-3') or a non-targeting hairpin (ShNT, target sequence 5'--CAACAAGATGAAGAGCACCAA-3') were cloned into the pLKO.1 vector. Viral packaging was performed by plating $9x10^4$ HEK293T cells in 0.5mL media in 24 well plates. 24 hours later the calcium phosphate method was used to transfect 100ng pMDL-RRE, 35ng RSV-Rev, and 50ng CMV-Vsvg. Media was removed 24 hours after transfection and 300µL fresh media was added to concentrate the virus. Supernatants containing viral particles were collected 20-24 hours after the media change. Supernatants for each line were pooled and spun for 5minutes at 4000 rpm to remove any cellular debris. 100µl viral supernatant was added to $1.5x10^5$ wild type Jurkat T cells in 24-well plates to bring the final volume to 300µL. 24 hours after infection, infected cells for each line were pooled, spun for 5 minutes at 1400 x *g*, and resuspended in fresh RPMI containing 0.5µg/mL puromycin and selected for 5 to 8 days. Knockdown was assessed by Western blot analysis using an anti-C9orf9 antibody. For rescue assays, cells were transfected with 1500ng IgK_2-IFN-Luc, 200ng pCSK-LacZ, the inidicated amounts of pULTRA rescue construct, and pcDNA3 empty expression vector such that the total DNA transfected was 3µg. The pULTRA expression vector (Addgene Plasmid #24129) contains a human Ub promoter upstream of GFP and a multicloning region that can be used to create a pseudo-polycistronic vector where inserted constructs are separated by viral 2A sequences which allow for ribosomal skipping and the simultaneous expression of multiple inserts. Rescue assays were conducted with a

construct which contains GFP-P2A-long C9orf9-T2A-short C9orf9 in which both versions of C9orf9 are sh5-resistant. Cells were transfected with LT1 as described above, and luciferase activity was assessed as in previous experiments.

Detection of endogenous PKC θ phosphorylation, and IκBα phosphorylation and degradation

$1x10^6$ Jurkat T cells were stimulated with 1μg/mL each anti-human CD3, anti-human CD28, and anti-mouse IgG1 in a final volume of 1mL in 48 well plates for the indicated times. Cells were harvested and kept on ice for at least 5 minutes to quench the reaction. The samples were spun for 5 min at 5000rpm at 4°C to pellet cells. Cells were then lysed in 50μL IP Lysis Buffer plus 2.5mM sodium orthovanadate, 10mM sodium fluoride, and 10mM β-glycerophosphate. Cells were incubated on ice for 10 minutes, then spun for 5 minutes at MAX rpm 4°C to pellet debris. 20μL lysate was boiled in the presence of SDS-PAGE loading buffer and resolved on 12% SDS-PAGE before being transferred to PVDF membrane. Membranes were analyzed by Western blot using mouse anti-Phospho-IκBα (Cell Signaling Technology, Inc. 9246S), rabbit anti-IκBα (Sigma sc-371), rabbit anti-C9orf9 (Sigma HPA022243), rabbit anti-GAPDH (Cell Signaling 5174P), goat anti-PKCθ (Santa Cruz sc-1875), rabbit anti-phospho PKCθ T538 (Cell Signaling 9377), rabbit anti-LAT (Cell Signaling 9166), and rabbit anti Phospho-LAT (Cell Signaling 3581). Images were quantitated using ImageJ.

OCI-Ly3 infection and survival assay

Virions containing the pSUPER.retro.neo+GFP (pSRGN, Oligoengine) vector with C9orf9 shRNA and packaged with pCL-Eco were made in 293T cells as previously described [10] and used to infect OCI-Ly3 cells expressing the ecotropic receptor mCAT1. A non-target shRNA was used as a negative control (sense sequence 5'-CAACAAGATGAAGAGCACCAA-3', loop sequence 5'-CTCGAG-3') and an shRNA targeting CARD11 (Sense sequence, 5'-TGGTCAAGAAGCTGACGATTC-3', loop sequence 5'-TTCAAGAGA-3') was used as a positive control. C9orf9 was targeting using the same shRNA as in Jurkat experiments, but designed for pSRGN (sense sequence 5'-AGAGCTACATGAACACTACT-3', loop 5'-TTCAAGAGA-3'). Retroviral packaging was performed in HEK 293T cells. $5x10^5$ cells were plated in 2mL complete DMEM. 24 hours after plating 800ng pCL-Eco and 3200ng pSRGN vector were transfected using 10µL Lipofectamine 2000 (ThermoFisher) and 250µL Opti-MEM media. 24 hours post transfection the DMEM was removed and replaced with 1.5mL OCI medium, which is Iscove's modified Dulbecco medium (IMDM) supplemented with 20% human serum (Atlanta Biologicals S40110), 50 U/mL each of penicillin and streptomycin and 55µM β-mercaptoethanol. OCI-Ly3 cells were plated at $4x10^5$ cells/mL in 500µL OCI media. Viral supe was collected and debris spun out by centrifugation. 500µL viral supe was added to OCI-Ly3 cells as well as polybrene to ao final concentration of 3µg/mL. 18-24 hours after infection, cells were spun down and resuspended in 1.5mL OCI media. 1mL additional OCI media was added 24 hours later.

3 days after infection, the percent of GFP positive cells was determined by flow cytometry on a BD LSRII and measurements were taken every three days thereafter.

CRISPR Mouse

Generally, the methodology of the Jaenisch group was used to generate the Cas9 mRNA and specific sgRNA against C9orf9 [31]. Specifically, annealed oligos were inserted into the PX330 vector (forward 5'- CACCGACTTCTGCTCGATGCTGCGG-3', reverse 5'-AAACCCGCAGCATCGAGCAGAAGTC-3'). The target region was amplified by PCR. RNA was generated using the HiScribe T7 Quick High Yield Synthesis Kit (NEB E2050) and purified using the MEGAclear Transcription Clean-up Kit (ThermoFisher/Ambion AM1908). A T7 transcription start site was inserted into PX330 upstream of Cas9 to aid in Cas9 synthesis. The mMessage mMachine T7 kit (ThermoFisher/Ambion AM1344) to perform *in vitro* transcription to generate Cas9 mRNA and LiCl precipitation was performed for purification. The 126bp oligo HDR template was ordered from IDT (Coralville, IA) at the 4nM scale and with standard desalting (5'-GCTCCAGAGCCGCAATGAAGGTGAACTGTTGCTGCTGGAAGAGCTTATACTTCTGCTCGACCTAGGTGCTGCGGAGGGACTCTTTCACCTCATTCATTGTTGCTCTTAGGTCTCACAGGACAGAAA-3'). The injection mixture contained 25ng/µL (2µg total) Cas9 mRNA, 1µg sgRNA, and 2µg DNA oligo in 80ul H_2O and was injected into single cell C57/Black 6 embryos by the JHMI Transgenic Mouse Core.

Pups from the resultant embryos were genotyped by amplifying a 640bp region of Chromosome 2 (forward primer: 5'- GCAGTGGTGAACAACTCGAAGGAC -3',

reverse primer: 5'- GTGGGGAAACTGAGGCGTAGTG -3') using the Roche FastStart Taq kit #04738357001 and digesting overnight with AvrII (NEB).

Western blotting of mouse testes:

Mouse testes from WT C57/B6 and C9orf9 KO mice were harvested, lysed in IP Lysis Buffer plus protease inhibitor cocktail as described above, and protein was quantitated by Bradford reagent (BioRad). 20ug total protein per lane was boiled in the presence of 3X SDS Sample Buffer and run on 12% SDS-PAGE. Protein was transferred to PVDF and membranes probed for C9orf9 (Sigma HPA022243) and GAPDH (Cell Signaling 5174P).

Flow Cytometry of Mouse B and T cells

Mouse splenocytes, thymocytes, and bone marrow tissue was separated into single cell suspensions. Red blood cells were lysed in ACK buffer (Quality Biologicals). Lymphocytes were resuspended in complete RPMI as described in the Jurkat cell protocol. Miltenyi MACS negative selection kits were used to isolate CD4+ T cells, CD8+ T cells, or Pan B cells following the manufacturer's instructions. For developmental studies, antibodies against CD3 (BD 553061), CD4 (BD 553730), CD8 (BD 563786), CD25 (BD 557192), CD44 (BD 560569), CD62L (BD 562910), B220/CD45R (BD 561880), CD19 (BD 557655), IgM (BD 553408), CD43 (BD 553271), CD23 (BE 553139), and CD21 (BD562797) were used. In CFSE experiments, cells were loaded with Invitrogen CellTrace CFSE. B cells were stimulated with 10µg/mL anti-IgM (ebioscience 16-5092-85) or 20 µg/mL LPS (Sigma L3012). T cells were stimulated using 3µg/mL plate bound anti-CD3 (BD clone 3751) and 2µg/mL soluble anti-CD28 (BD clone 145-2c11). Unstimulated samples were incubated in media only. Proliferation

was measured after 72 hours incubation at 37°C in 5% CO_2 and 95% humidity. Upregulation of surface activation markers was measured after 24 hours of stimulation using antibodies against CD25 (BD557192), CD86 (Biolegend 105031), MHC Class II I^{ab} (Biolegend 116419), CD69 (BD 553236), and CD44 (BD 560569) [36, 37]. Stains involving B cell surface markers were performed in the presence of FcR blocking using TruStain FcX (Biolegend 101320). Cytometry was performed on a BD LSRII and analyzed in FlowJo.

Chapter 3: Discussion

The role of C9orf9 in antigen receptor signaling

Regulated antigen receptor signaling is critical for controlling the adaptive immune response. Antigen receptor pathways are highly complex networks that must receive, integrate, transmit, and then interpret signals in the correct pro- or anti-inflammatory action. While much is known about the initial and final steps of TCR/BCR-to-NF-κB signaling, much remains to be clarified about the intervening steps.

In order to identify previously unknown members of the TCR- and BCR-to-NF-κB pathways, a high throughput protein-protein interaction screen was conducted using isolated, recombinant CARD11 and protein expression chips. C9orf9 was identified as a potential interactor of CARD11 and further investigated for its ability to enhance CARD11 signaling. Although the interaction with CARD11 was never confirmed, C9orf9's ability to interact with the CARD11 cofactor Bcl10 helped clarify its ability to enhance CARD11 signaling.

Many questions still remain about the mechanism of C9orf9 activity. Tests of C9orf9 truncation constructs in the 293T cell NF-κB luciferase reporter assay indicate that there may be a region between amino acids H165 and Q189 in the long form of C9orf9 that acts as an inhibitory region and prevents it from interacting with Bcl10 and other cofactors. Alternatively, there may be an activating region between amino acids Q189 and K206 in the long isoform which is required for C9orf9 interaction with Bcl10 and activation of the pathway. Further truncation studies could help clarify which of these two hypotheses is correct. Additionally, the rescue experiments in C9orf9 knockdown Jurkat T cells should be conducted with constructs that express the truncated

versions of long C9orf9 and the full length short version of C9orf9. This is the best way to determine which residues of the long form are required for activity in endogenous settings.

One of the challenges of this work was attempting to place C9orf9 epistatically in the antigen receptor pathway. The data was in some ways contradictory, showing a greater effect of C9or9f knockdown upstream of CARD11 and Bcl10, at PKCθ and LAT, than the effect seen down stream of CARD11 at IκBα. A few hypotheses are plausible from the current data. C9orf9's two isoforms may act in different places in the pathway, which seems to be the most plausible explanation for why both isoforms are required for signaling. Preliminary evidence does not indicate that the two isoforms interact with each other in a complex, or that they both interact with the same cofactors in the same time in the same way, although more detailed experiments would be required to confirm that they interact at the same "step" of the pathway, the CBM complex, but with different complex members simultaneously. Rather, it seems more likely that one form interacts at the level of the CBM complex and the other isoform interacts upstream of CARD11, at or above LAT.

Alternatively, the unexpected change in LAT and PKCθ phosphorylation could be due to a feedback loop, where the C9orf9 isoforms act at the level of CARD11 and Bcl10, but changing levels of NF-κB activation feedback on to the same cells and prevent them from responding as well to antigen receptor stimulation as cells which have more successfully initiated NF-κB dependent transcription programs. The existence of a feedback loop seems plausible because of the non-linear relationship between CARD11

expression and cellular activity. One challenge of the C9orf9 truncation experiments in 293T cells was getting equivalent expression of both C9orf9 and CARD11 across experiments. The C9orf9 truncation constructs express at different levels in 293Ts, which is reasonable and consistent for these types of experiments and constructs. Preliminary experiments were conducted to determine which nanogram amounts of C9orf9 constructs gave equivalent levels of protein expression. However, once these nanogram amounts were cotransfected into 293Ts with 30ng of CARD11, their expression changed. For some constructs, co-expression with CARD11 increased C9orf9 expression. Expression of the full length long form of C9orf9 also increased CARD11 expression, which interestingly correlated with that sample having the highest activation of the luciferase reporter of all the conditions tested in that assay. This discrepancy in protein expression levels makes it difficult to interpret the degree to which the long form of C9orf9 enhances CARD11 signaling relative to other C9orf9 constructs. However, it does suggest that activation of CARD11 initiates a transcription program which in turn upregulates CARD11 itself, allowing for even greater activation of the luciferase reporter. This feedback loop would explain the discrepancies seen in LAT and PKCθ phosphorylation in C9orf9 KD Jurkats when compared to control cells.

A third explanation for this unexpected result involves our current understanding of PKCθ placement in the antigen receptor pathway. It is possible that PKCθ acts at multiple steps in the pathway, and not only at its currently understood placement upstream of CARD11 at the immunological synapse. Interestingly, C9orf9 KD Jurkat T cells stimulated with PMA/ionomycin do display defective signaling in the luciferase

reporter assay but did not display a defect in PKCθ phosphorylation. One complication of this result is that the mechanism of action of PMA/ionomycin stimulation is not entirely clear. It is thought that PMA may act on PKCθ, but it is also thought to act at other, unspecified places in the pathway. Because the exact step(s) of action of PM are unknown, it is difficult to explain where PKCθ may be acting or why these inconsistent results are seen in C9orf9 KD Jurkats.

Separating the functions of the two isoforms of C9orf9

The major obstacle of this project was dealing with the presence of two different isoforms of C9orf9. Because of the orientation of the exons and the location of the splice site that generates the short isoform, the entire mRNA transcript of the short isoform is contained within the transcript of the long isoform. Because shRNA targets mRNA transcripts, it is impossible to use this technology to specifically knockdown the short isoform. While it was possible to specifically target the long isoform using shRNA, I did not spend much time pursuing the specific function of the long isoform because the long C9orf9 KD Jurkats did not have as strong of a phenotype in the NF-κB luciferase reporter assay as the dual C9orf9 KD cells. It would be worth pursuing the long isoform specific knockdown phenotype to try to understand the specific function of the long isoform.
A similar problem was encountered when designing CRISPR/Cas9-mediated knockdown of C9orf9 in mice. Because CRISPR targets DNA, any intact code will be transcribed and potentially translated into protein. It is therefore important to target a region within a few codons of the translational start site. The structure of the C9orf9 locus and the 165 N-terminal amino acids which are shared between the two isoforms make it impossible to

use CRISPR to target one isoform specifically. Again, it will be extremely difficult to characterize the mechanism of action of C9orf9 without being able to specifically knockdown one isoform and isolate its contribution to C9orf9 function. As technology changes, scientists interested in pursuing studies of C9orf9 function should pay attention to new developments in gene expression modification and apply new technologies to the problem of C9orf9 isoform specific knockdown.

Further studies in the C9orf9 KO mouse model

Several potential phenotypes were examined in the C9orf9 KO mice. Basic development of B and T cells were analyzed and found to be normal. Upregulation of activation in markers in B and T cells in response to stimulation was also normal, as was the ability of those cells to proliferate under stimulation. Because of the phenotype present in C9orf9 KD Jurkat T cells, I expected to find a defect in B or T cell development or basic activation. None of the expected defects were present. There are, however, many other potential phenotypes in the KO mice which were not examined. These more complex *in vivo* models include tests of the ability to respond to T-dependent vs T-independent antigens, tumor challenge models, vaccine titer tests, and NK cell killing ability. Tests of any of these functions could reveal an important role for C9orf9 in the adaptive and innate immune systems. Finally, the imbalance in the Mendelian ratio of pups born to het-het crosses suggests a potential neural tube defect like that seen in the Bcl10 KO mice. Timed matings and examination of fetal development would confirm the hypothesis that C9orf9 works with Bcl10 in prenatal neural development.

References

1. Pahl HL. Activators and target genes of Rel/NF-kappaB transcription factors. Oncogene. 1999. 18(49):6853-66.
2. Vallabhapurapu S., and Karin M. Regulation and Function of NFkappaB Transcription Factors in the Immune System. Annual Review of Immunology. 2009. 27:693-733.
3. Pomerantz J.L., Denny E.M., and Baltimore D. CARD11 mediates factor-specific activation of NF-{kappa}B by the T cell receptor complex. EMBO J. 2002. 21(19):5184-5194.
4. Hara H., Wada T., Bakal C , Kozieradzki I., Suzuki S., Suzuki N., Nghiem M., Griffiths E.K., Krawczyk C, Bauer B., et al. The MAGUK family protein CARD11 is essential for lymphocyte activation. Immunity. 2003. 18(6):763-775.
5. Egawa T., Albrecht B., Favier B., Sunshine M.J., Mirchandani K., O'Brien W., Thome M., and Littman D.R. Requirement for CARMAl in antigen receptor-induced NF-kappa B activation and lymphocyte proliferation. Curr Biol. 2003. 13(14):1252-1258.
6. Sommer K, Guo B, Pomerantz JL, Bandaranayake AD, Moreno-García ME, Ovechkina YL, Rawlings DJ. Phosphorylation of the CARMA1 linker controls NF-B activation. Immunity. 2005. 23(6):561-574.
7. Shinohara H, Maeda S, Watarai H, Kurosaki T. IkappaB kinase beta-induced phosphorylation of CARMA1 contributes to CARMA1 Bcl10 MALT1 complex

formation in B cells. The Journal of Experimental Medicine. 2007. 204(13):3285-93.

8. Lin X, Wang D. The roles of CARMA1, Bcl10, and MALT1 in antigen receptor signaling. Seminars in Immunology. 2004. 16(6):429-35.
9. McCully R.R., and Pomerantz J.L. The protein kinase C-responsive inhibitory domain of CARD 11 functions in NF-kappaB activation to regulate the association of multiple signaling cofactors that differentially depend on Bcl10 and MALT1 for association. Mol Cell Biol. 2008. 28(18):5668-5686.
10. Chan W, Schaffer TB, Pomerantz JL. A quantitative signaling screen identifies CARD11 mutations in the CARD and LATCH domains that induce Bcl10 ubiquitination and human lymphoma cell survival. Mol Cell Biol. 2013. 33(2):429-43
11. Wu CJ, Ashwell JD**.** 2008. NEMO recognition of ubiquitinated Bcl10 is required for T cell receptor-mediated NF-kappaB activation. Proc. Natl. Acad. Sci. U. S. A. 2008. 105(8):3023–3028.
12. Matsumoto R, Wang D, Blonska M, Li H, Kobayashi M, Pappu B, Chen Y, Lin X. 2005. Phosphorylation of CARMA1 plays a critical role in T cell receptor-mediated NF-kappaB activation. Immunity. 2005. 23(6):575–585.
13. Thome M, Charton JE, Pelzer C, Hailfinger C. Antigen receptor signaling to NF-kappaB via CARMA1, BCL10, and MALT1. Cold Spring Harb. Perspect. Biol. 2010. 2(9):a003004.

14. Wegener E, Oeckinghaus A, Papadopoulou N, Lavitas L, Schmidt-Supprian M, Ferch U, Mak TW, Ruland J, Heissmeyer V, Krappmann D. Essential role for IkappaB kinase beta in remodeling Carma1-Bcl10-Malt1 complexes upon T cell activation. Mol. Cell. 2006. 23(1):13–23.
15. Smith-Garvin J.E., Koretzky G.A., and Jordan M.S. T Cell Activation. Annual Review of Immunology. 2009. 27:591-619.
16. Weiss A., and Littman D.R. Signal transduction by lymphocyte antigen receptors. Cell. 1994. 76(2):263—274.
17. Chan A.C., Irving B.A., Fraser J.D., and Weiss, A. The zeta chain is associated with a tyrosine kinase and upon T-cell antigen receptor stimulation associates with ZAP-70, a 70-kDa tyrosine phosphoprotein. Proc Natl Acad Sci USA. 1991. 88(20):9166-9170.
18. Oh-hora M., and Rao A. Calcium signaling in lymphocytes. Curr Opin Immunol. 2008. 20(3):250-258.
19. Reth M. Antigen receptor tail clue. Nature. 1989. 338(6214):383–4.
20. Liu W, Meckel T, Tolar P, Sohn HW, Pierce SK. Antigen affinity discrimination is an intrinsic function of the B cell receptor. J.Exp.Med. 2010. 207(5):1095–111.
21. So L, Fruman DA. PI3K signaling in B- and T-lymphocytes: new developments and therapeutic advances. Biochem J. 2012. 442(3):465-81
22. The Non-Hodgkin's Lymphoma Classification Project. A Clinical Evaluation of the International Lymphoma Study Group Classification of Non-Hodgkin_s Lymphoma. Blood. 1997. 89(11): 3909-3918.

23. Rosenwald A, Wright G, Chan WC, Connors JM, Campo E, Fishe RI, Gascoyne RD, Muller-Hermelink HK, Smeland EB, Giltnane JM, Hurt EM, Zhao H, Averett L, Yang L, Wilson WH, Jaffe ES, Simon R, Klausner RD, Powell J, Duffey PL, Longo DL, Greiner TC, Weisenburger DD, Sanger WG, Dave BJ, Lynch JC, Vose J, Armitage JO, Montserrat E, López-Guillermo A, Grogan TM, Miller TP, LeBlanc M, Ott G, Kvaloy S, Delabie J, Holte H, Krajci P, Stokke T, Staudt, Louis M. The use of molecular profiling to predict survival after chemotherapy for diffuse large-B-cell lymphoma. The New England Journal of Medicine. 2002. 346(25):1937-47
24. Davis RE, Brown KD, Siebenlist U, Staudt LM. Constitutive nuclear factor kappaB activity is required for survival of activated B cell-like diffuse large B cell lymphoma cells. The Journal of Experimental Medicine. 2001. 194(12):1861-74.
25. Lenz G, Davis RE, Ngo VN, Lam L, George TC, Wright GW, Dave SS, Zhao H, Xu W, Rosenwald A, Ott G, Muller-Hermelink HK, Gascoyne RD, Connors JM, Rimsza LM, Campo E, Jaffe ES, Delabie J, Smeland EB, Fisher RI, Chan WC, Staudt LM. Oncogenic CARD11 mutations in human diffuse large B cell lymphoma. Science. 2008. 319(5870):1676-9.
26. Snow AL, Xiao W, Stinson JR, Lu W, Chaigne-Delalande B, Zheng L, Pittaluga S, Matthews HF, Schmitz R, Jhavar S, Kuchen S, Kardava L, Wang W, Lamborn IT, Jing H, Raffeld M, Moir S, Fleisher TA, Staudt LM, Su HC, Lenardo MJ. Congenital B cell lymphocytosis explained by novel germline CARD11 mutations. J Exp Med. 2012. 209(12):2247-61.

27. Masson C, Parisot M, Zhang Y, Matthews HF, Su HC, Durandy A, Fischer A, Kracker S, Snow AL. Mild B-cell lymphocytosis in patients with a CARDD11 C49Y mutation. J Allergy Clin Immunol. 2015. 136(3):819-821.
28. Brohl AS, Stinson JR, Su HC, Badgett T, Jennings CD, Sukumar G, Sindiri S, Wang W, Kardava L, Moir S, Dalgard CL, Moscow JA, Khan J, Snow AL. Germline CARD11 Mutation in a Patient with Severe Congenital B Cell Lymphocytosis. J Clin Immunol. 2014 Oct 29. [Epub ahead of print].
29. Morin RD, Mendez-Lago M, Mungall AJ, Goya R, Mungall KL, Corbett RD, et al. Frequent mutation of histone-modifying genes in non-Hodgkin lymphoma. Nature. 2011. 476(7360):298–303.
30. Cheng J, Montecalvo A, Kane LP. Regulation of NF-κB induction by TCR/CD28. Immunol Res. 2011. (50(2-3): 113-7.
31. Wang H, Yang H, Shivalila CS, Dawlaty MM, Cheng AW, Zhang F, Jaenisch R One-step generation of mice carrying mutations in multiple genes by CRISPR/Cas-mediated genome engineering. Cell. 2013. 153(4):910-8
32. Zeng H, Chen Y, Yu M, Xue L, Gao X, Morris SW, Wang D, Wen R. T cell receptor-mediated activation of CD4+CD44hi T cells bypasses Bcl10: an implication of differential NF-kappaB dependence of naïve and memory T cells during T cell receptor-mediated responses. J Biol Chem. 2008. 283(36):24392-9.
33. Nagasawa T. Microenvironmental niches in the bone marrow required for B-cell development. Nat Rev Imm. 2006. 6(2):107-16.

34. Xue L, Morris SW, Orihuela C, Tuomanen E, Cui X, Wen R, Wang D. Defective development and function of Bcl10-deficient follicular, marginal zone, and B1 B cells. Nat Immunol. 2003. 4(9):857-65.

35. Chu Y, Vahl JC, Kumar D, Heger K, Bertossi A, Wójtowicz E, Soberon V, Schenten D, Mack B, Reutelshöfer M, Beyaert R, Amann K, van Loo G, Schmidt-Supprian M. B cells lacking the tumor suppressor TNFAIP3/A20 display impaired differentiation and hyperactivation and cause inflammation and autoimmunity in aged mice. Blood. 2011. 117(7):2227-36.

36. Chu Y, Soberon V, Glockner L, Beyaert R, Massoumi R, van Loo G, Krappmann D, Schmidt-Supprian M. A20 and CYLD do not share significant overlapping functions during B cell development and activation. J Immunol. 2012. 189(9):4437-43.

37. Ruland J, Duncan GS, Elia A, del Barco Barrantes I, Nguyen L, Plyte S, Millar DG, Bouchard D, Wakeham A, Ohashi PS, Mak TW. Bcl10 is a positive regulator of antigen receptor-induced activation of NF-κB and neural tube closure. Cell. 2001 Jan 104(1):33-42.

38. Condie, B. G., A. H. Brivanlou, and R. M. Harland. 1990. Most of the homeobox-containing Xhox 36 transcripts in early *Xenopus* embryos cannot encode a homeodomain protein. Mol. Cell. Biol. 10:3376–3385.

CURRICULUM VITAE FOR Ph.D. CANDIDATES

The Johns Hopkins University School of Medicine

deMauri S. Mackie

February 2016

Educational History:

Ph.D.	2016	Program in Cellular and Molecular Medicine Mentor: Joel Pomerantz, Ph.D.	Johns Hopkins School of Medicine
B.A.	2006	Biochemistry Minors in German and Psychology	University of Pennsylvania

Other Professional Experience:

Research Technician	2006-2008	Beckman Center for Immune Monitoring and Lab of W. Martin Kast, Ph.D. University of Southern California
Research Assistant	2005-2006	Lab of Laurie Kilpatrick, PhD. Children's Hospital of Philadelphia
Research Assistant	2004	Lab of Philip Cohen, M.D. University of Pennsylvania
Research Assistant	2003-2004	Lab of Ivan Dmochowski, Ph.D. University of Pennsylvania

Scholarships, Fellowships, or other external funding

Ruth L. Kirschstein National Research Service Award (NRSA), National Cancer Institute, National Institutes of Health. F31 CA171532 "Identifying Regulators of Oncogenic CARD11 in Diffuse Large B Cell Lymphoma," April 2013-March 2016. Stipend support.

Publications, Peer-Reviewed

Pedersen SM, Chan W, Jattani RP, **Mackie dS**, and Pomerantz JL: Negative Regulation of CARD11 Signaling and Lymphoma Cell Survival by the E3 Ubiquitin Ligase RNF181. Mol Cell Biol. 2015 Dec 28. pii: MCB.00876-15. PMID: 26711259

Korchak, H.M., Dorsey, L.B., Li, H., **Mackie, deM**., and Kilpatrick, L.E.: Selective roles for α-PKC in positive signaling for O_2^- generation and calcium mobilization but not elastase release in differentiated HL-60 cells. Biochim Biophys Acta. 2007 Mar;1773(3):440-9. PMID: 17157935

Kilpatrick, L.E., Sun, S., **Mackie, deM**., Baik, F., Li, H. and Korchak, H.M: Regulation of TNF mediated anti-apoptotic signaling in human neutrophils: role of δ-PKC and ERK1/2. J Leukoc Biol. 2006 Dec;80(6):1512-21. Erratum in: J Leukoc Biol. 2008 Mar;83(3):797. PMID: 17138860

Service and Leadership

Teaching Experience

2012 Teaching Assistant, Scientific Foundations of Medicine: Metabolism, Johns Hopkins University School of Medicine

2011 Teaching Assistant, Topics in Cellular and Molecular Medicine, Johns Hopkins University School of Medicine

Scientific Mentorship Experience

Mentorship of first year graduate students during their 10 week rotations in the Pomerantz lab

2015 Mary Soliman

2013 Varenka Rodriquez

2013 Donna Dang

2012 Iris Chen

Volunteer Experience

2013 Executive Team Human Resource Officer, Thread (Formerly Incentive Mentoring Program)

2012-2013 Executive Team Human Resource Officer Trainee, Thread

2011-2012 Chair of Volunteer Services, Thread

2009-2011 Co-Director of Recruitment, Thread

2008-2014 Mentor, Thread